NASA CR-114622
Available to the Public

DESIGN INTEGRATION AND NOISE STUDIES FOR JET STOL AIRCRAFT

Task VIIC
Augmentor Wing Cruise Blowing Valveless System

Volume I—Static Testing of Augmentor Noise and Performance

by J. M. Campbell, D. L. Harkonen, J. V. O'Keefe

November 1973

Distribution of this report is provided in the
interest of information exchange. Responsibility
for the contents resides in the author or
organization that prepared it.

Prepared under Contract NAS2-6344 by

BOEING COMMERCIAL AIRPLANE COMPANY
P. O. Box 3707
Seattle, Washington 98124

for

Ames Research Center
NATIONAL AERONAUTICS AND SPACE ADMINISTRATION

1. Report No. NASA CR-114623	2. Government Accession No.	3. Recipient's Catalog No.
4. Title and Subtitle Design Integration and Noise Studies For Jet STOL Aircraft; Task VIIC; Volume I—Static Testing of Augmentor Noise and Performance		5. Report Date November 1973
		6. Performing Organization Code
7. Author(s) J. M. Campbell, D. L. Harkonen, and J. V. O'Keefe		8. Performing Organization Report No. D6-41216
		10. Work Unit No.
9. Performing Organization Name and Address Boeing Commercial Airplane Company P.O. Box 3707 Seattle, Washington 98124		11. Contract or Grant No. NAS2-6344
		13. Type of Report and Period Covered Contractor Report
12. Sponsoring Agency Name and Address National Aeronautics and Space Administration Washington, D.C. 20546		14. Sponsoring Agency Code

15. Supplementary Notes

16. Abstract

Static performance and acoustic tests were conducted on a two-dimensional one-third-scale augmentor flap model that simulated a cruise blowing augmentor system designed for a 150-passenger STOL airplane. The cruise blowing augmentor, which offers a degree of simplicity by requiring no fan air diverter valves, was simulated by fitting existing lobe suppressor nozzles with new nozzle fairings. Flow turning performance of the cruise blowing augmentor was measured through a large range of flap deflection angles. The noise suppression characteristics of a multilayer acoustic lining installed in the augmentor were also measured.

17. Key Words (Suggested by Author(s)) Augmentor wing Jet STOL Noise Suppression	18. Distribution Statement Unclassified—unlimited		
19. Security Classif. (of this report) Unclassified	20. Security Classif. (of this page) Unclassified	21. No. of Pages 45	22. Price* 5.25

CONTENTS

DESIGN INTEGRATION AND NOISE STUDIES

FOR JET STOL AIRCRAFT

Volume I—Static Testing of
Augmentor Noise and Performance

By J. M. Campbell, D. L. Harkonen, J. V. O'Keefe

1.0 INTRODUCTION AND SUMMARY

The objective of the Design Integration and Noise Study Program is to develop, through analysis, static and wind tunnel testing, and design integration studies, an augmentor wing jet flap configuration for a jet STOL transport aircraft having maximum propulsion and aerodynamic performance with minimum noise generation. The augmentor installations studied in tasks III and V, as described in references 1, 2, and 3, are based on the concept that fan bypass air is directed to the augmentor nozzles only during takeoff and approach. Through a system of diverter valves, the fan exhaust is directed to an engine nozzle during the cruise mode. The augmentor nozzles in this design are located within the normal wing envelope.

Eliminating the requirement for diverter valves and separate cruise nozzles is accomplished by locating the augmentor nozzles outside the wing envelope. The augmentor nozzles then provide thrust during all modes of operation. This concept is illustrated in figure 1. The fan air is directed to the wing ducts, with a portion used for leading edge and aileron blowing. The major part of the air discharges from multielement lobed nozzles through acoustically lined flaps during the takeoff and approach modes. In the cruise mode, the flaps are retracted, and the air blows over the upper surface of the shroud.

The static performance and acoustic data measured with the cruise blowing augmentor model and scaled for a range of flap chord lengths and duct losses demonstrate that a static thrust augmentation ratio of 1.2 is available for takeoff and that a cruise blowing augmentor system can be designed to achieve a 500-ft sideline noise level of 90 PNdB.

Inherent in the cruise blowing concept is a limitation on the angle that the augmentor nozzles can be canted down and still conform to the wing contour. This results in greater turning for a given flap angle and causes some augmentation loss.

As reported in reference 3, the task V static performance and acoustic tests, a maximum noise level at the 500-ft sideline of 95.6 PNdB was demonstrated for takeoff conditions. A static thrust augmentation of 1.32 was measured at the takeoff flap setting. These acoustic and performance levels were achieved with a corrugated splitter lobe nozzle (array area ratio = 8) and by use of multilayer tuned acoustic linings that were designed to attenuate task III multirow lobe nozzle noise.

Acoustic lining

4 +   2

Takeoff position

Nozzles

70% C

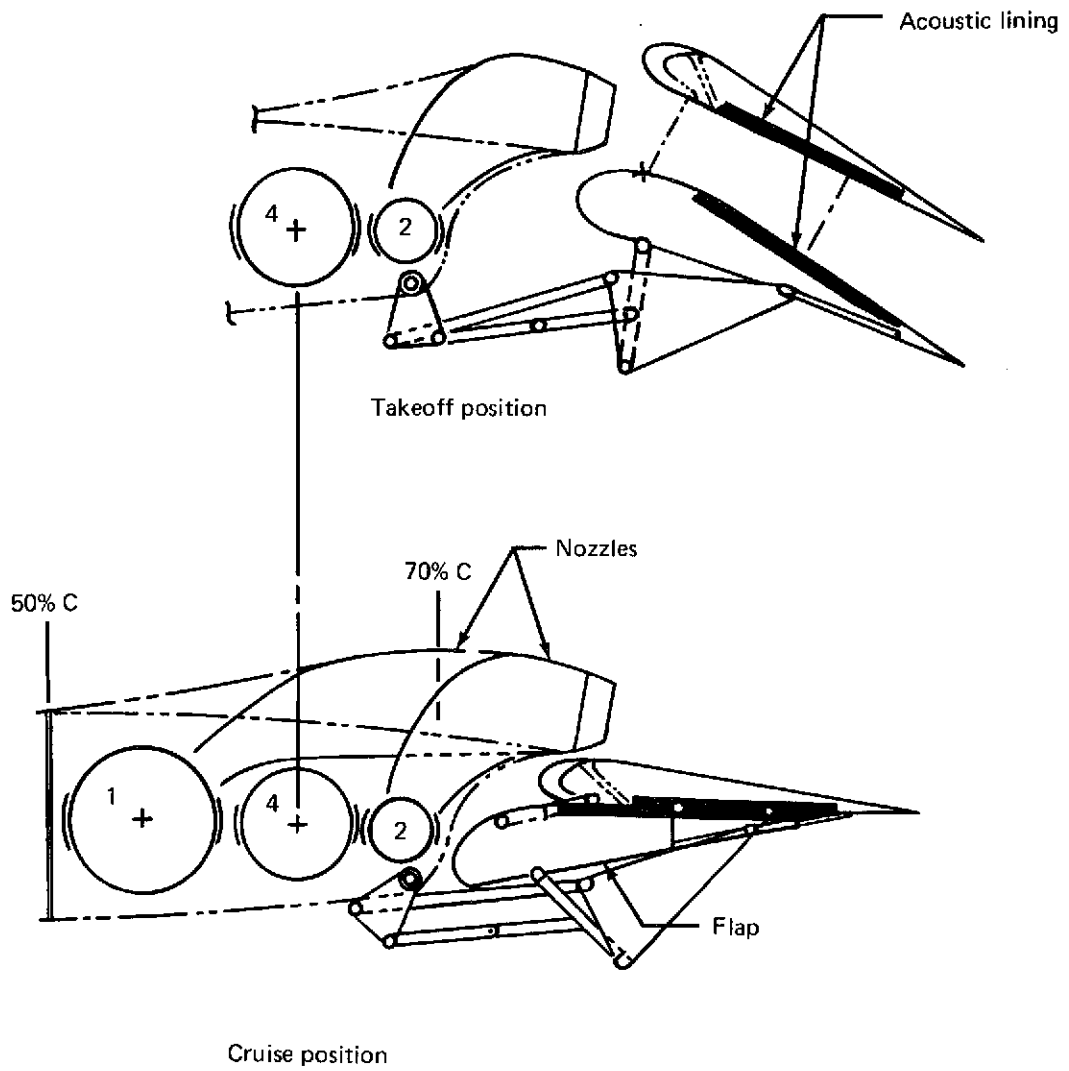50% C

1 +   4 +   2

Flap

Cruise position

FIGURE 1.—AUGMENTOR WING CRUISE BLOWING FLAP CONCEPT

Work reported here describes the additional evaluation of static thrust performance and noise levels measured with an augmentor representing a cruise blowing system using multilayer acoustic lining specifically designed to attenuate the corrugated lobe nozzle noise spectrum.

The static thrust augmentation ratios as a function of augmentor flow turning angle measured with the cruise blowing augmentor model are presented in figure 2. The levels are derived from test data, and they include the losses resulting from augmentor primary flow heating and flap acoustic lining. A reduction in thrust augmentation as the flow turning is increased is indicated in figure 2.

The single set of hardware available for this task did not permit optimization of design variables. There are several areas in the augmentor system that hold potential for improving the cruise blowing augmentor static turning performance. These include increasing the flap leading edge radius, reducing nozzle array height, revising nozzle exit shape, and changing nozzle fairing contour. Variations in these areas would have to consider stowage constraints and tradeoffs in noise and weight.

A new augmentor lining set, lining IV, was designed and fabricated for this task. Suppression characteristics are shown in figure 3. The measured difference between the unlined and lined augmentor was 4.6 PNdB; the predicted difference was 7.6 PNdB. The cause of this discrepancy was traced to the inability to measure the polyimide, glass lining material acoustic impedance accurately above 6.3 kHz. "Data" for the lining design procedure was derived by extrapolating impedance data above this frequency. The test evidence indicates that the impedance of the lining is much lower than predicted by the extrapolation. With this new information, the optimum scale model could be established by testing several linings which encompass the required impedance. However, this additional testing would have been beyond the scope of the program. The design of full scale (200,000 lb TOGW) lining could be done without further testing because frequencies above 6.3 kHz are relatively unimportant to PNL suppression.

In previous testing, the peak 500-ft sideline noise level was assumed to lie in the Beta = 60° plane, (β = 0° is the plane of symmetry). In these tests, additional data was recorded in the Beta = 45° and Beta = 75° planes. While the slot nozzle and the suppressor nozzle without augmentor still peaked in the Beta = 60° plane, the suppressor in the augmentor peaked in the Beta = 75° plane. This effect holds for both the valve and valveless configurations and for both lined and unlined augmentors. The increase in noise level on the 500-ft sideline is 1 to 2 PNdB. This result implies that the aircraft sideline noise levels would be 1 to 2 PNdB higher than was previously reported. Since the "line of sight" from the observer to the aircraft during takeoff is only 15° from the plane of the augmentor system, the augmentor system is "obscured" or "shielded" by the near side augmentor system. For an observer located in the Beta = 60° plane, 1.5 PNdB would be added for the noise from the far-side noise source, however, the far-side source would be undetectable by an observer in the Beta =75° plane. Therefore, the net effect of the shift in directionality is negligible.

The thrust performance and acoustic noise levels as they affect tradeoffs in the airplane design are discussed in reference 4.
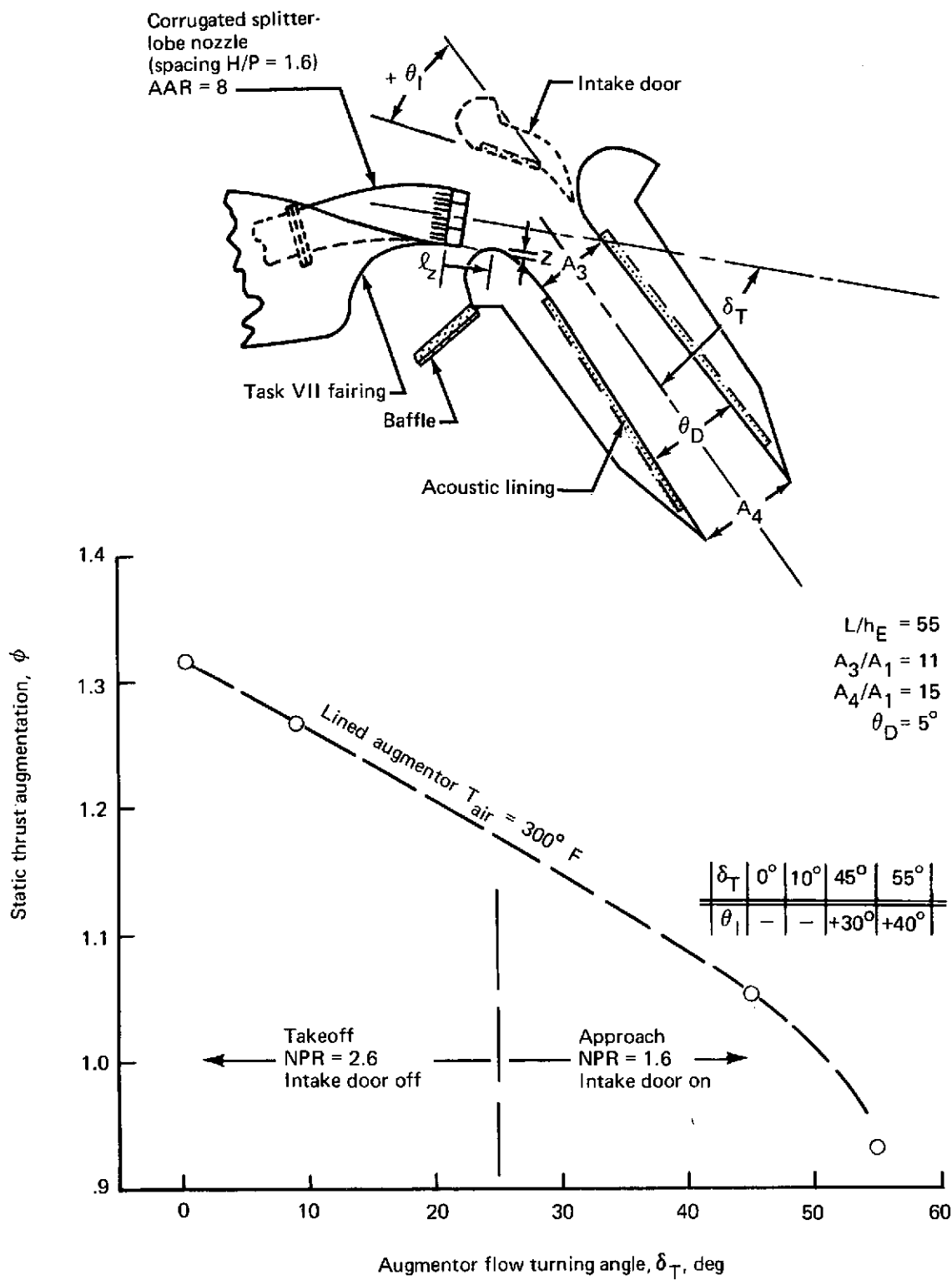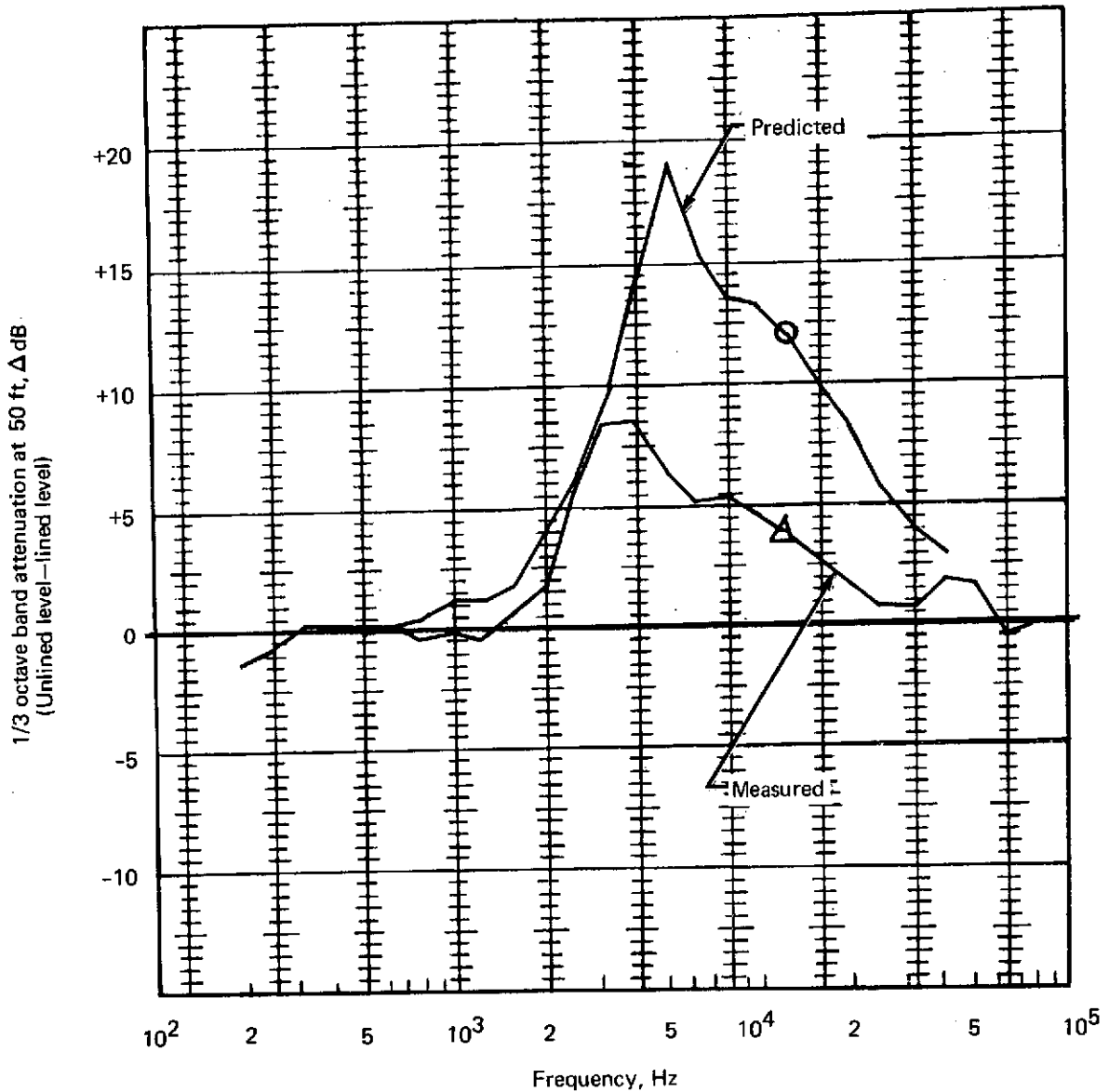
FIGURE 2.—CRUISE BLOWING AUGMENTOR FLOW TURNING PERFORMANCE

FIGURE 3.—COMPARISON OF PREDICTED AND MEASURED LINING ATTENUATION

2.0 SYMBOLS AND ABBREVIATIONS

A   area, sq in.

A^* blowing nozzle area at Mach 1.0, sq in.

AAR   augmentor primary nozzle array area ratio (ratio of the area bounded by the primary nozzle exits to the measured nozzle exit area)

$\cancel{A}$ wing aspect ratio

a   local velocity of sound, fps

b   augmentor span, in.

C   Correction factor (as a function of frequency), dB, or wing chord, in.

C_D nozzle discharge coefficient, measured airflow/ideal airflow

C_V nozzle velocity coefficient, measured thrust/(measured mass flow X ideal velocity)

D   diameter, in.

F   engine thrust or augmentor primary nozzle thrust, lb

FPR   fan pressure ratio

f   frequency, Hz

g   gravitational constant, fps^2

H   nozzle array height, in. ($H \equiv H_N = h_E \times AAR$)

H/P   nozzle height to spacing ratio

h   height, slot (or equivalent slot, $h_E = 0.432$ in.) $= \dfrac{\text{nozzle exit area}}{\text{model span b}}$, in.

L   augmentor length, in.

ℓ_Z distance along a parallel to the nozzle centerline from the nozzle exit plane to the flap tangent point (see fig. 10), in.

M   Mach number

MCR   cruise Mach number

m	airflow, slugs/sec (measured)
N	noy level, noys
NPR	nozzle pressure ratio
OASPL	overall sound pressure level, dB (re: 0.0002 microbar)
$OASPL_{max}$	maximum OASPL along a noise radiation line with respect to the jet axis, dB (re: 0.0002 microbar)
OBSPL	octave band sound pressure level, dB (re: 0.0002 microbar)
OEW	operating empty weight, lb
P	pressure, lb/sq in., nozzle pitch, in.
PNdB	unit of perceived noise level
PNL	perceived noise level, PNdB
PNL_{max}	maximum PNL along a noise radiation line with respect to the jet axis
q	dynamic pressure, lb/sq ft
R	impedance of a lining facing, cgs, rayls
RH	relative humidity, %
R^*	$R/\rho a$
R_N	Reynolds number
r	radius from nozzle exit to microphone (see fig. 4), ft
S, S_W	wing area, sq ft
S_N	Strouhal number (frequency x length)/velocity
SPL	sound pressure level, dB (re: 0.0002 microbar)
SR	slant range, ft
STOL	short takeoff and landing
T	temperature, °F,
T/O	takeoff power setting

TOGW	takeoff gross weight, lb
t	wing thickness, in.
V	velocity, fps
V_J	jet velocity, fps
W	airplane weight, lb
WCP	wing chord plane
w	lobe width, in.
Z	distance from lower edge of nozzle to tangent point on flap (see fig. 10), in.
α	air absorption (as a function of frequency), dB/1000 ft, airplane angle of attack, deg
β	plenum rotation or slot nozzle orientation with respect to flyover position, (see fig. 13), deg
δ_F	flap rotation angle with respect to WCP, deg
δ_N	augmentor primary nozzle deflection angle with respect to WCP, deg
δ_T	augmentor flap air turning angle, δ_F - δ_N, deg
θ	noise radiation angle with respect to thrust vector (see fig. 13), deg
θ_D	augmentor diffuser angle (see fig. 10), deg
θ_I	augmentor intake angle (see fig. 10), deg
λ	wavelength, ft
ρ	jet density, lb/cu/ft
ϕ	thrust augmentation ratio, flaps on thrust/flaps off thrust

Subscripts:

A	augmentor
b	span
D	diffuser

E	equivalent
F	flap (lower surface of augmentor), or fan
G	gross
I	ideal or intake
N	nozzle
RV	relative velocity
S	system or shroud
SD	standard day (59° F, 70% relative humidity
T	total (total pressure, total temperature)
X	extrapolation correction (noise)
1	augmentor primary
2	augmentor secondary
3	augmentor throat
4	augmentor exit

augmentor areas in plane perpendicular to flow axis

Superscripts:

—	average
	time rate

3.0 DISCUSSION

Previous work (ref. 1, 2, 5) developed the augmentor wing concept for a STOL airplane that produced a peak 500-ft sideline perceived noise level of 89 PNdB. System studies (ref. 3) and wind tunnel tests (ref. 6) have demonstrated the feasibility of the augmentor wing cruise blowing valveless design. The purpose of the static test program was to evaluate the augmentor performance and acoustic characteristics of the cruise augmentor design.

3.1 TEST FACILITY AND MODEL DESCRIPTION

In the paragraphs that follow, details of the test facility, test procedures, and instrumentation are discussed, as well as the accuracy and repeatability of performance and acoustic measurements.

3.1.1 Facility

The Boeing North Field Mechanical Laboratories in Seattle, Washington, were chosen for the test location. The laboratories have a facility especially suited for large-scale combined acoustic and thrust performance test programs. The augmentor thrust is measured with a six-component, platform-type balance bridged with high-pressure air; the noise can be measured in a $180°$ arc in an acoustic arena as shown in figures 4 and 5. The thrust stand accurately measures model forces using either heated ($300°$ F) or ambient-temperature nozzle air. Nozzle flow rates are determined with precision using ASME venturi flow meters calibrated against a Boeing standard nozzle. An acoustically treated muffler plenum, located on the balance platform upstream of the test nozzle plenum, prevents noise generated by the air supply lines and control valves from reaching the test nozzles.

To acquire acoustic data of the highest quality, data were recorded only during a limited range of atmospheric conditions. Because of the precision desired for acoustic measurements and the very large volume of acoustic data expected, each component of the instrumentation system for noise measurement was carefully chosen and integrated. The basic noise-measuring system consists of microphones, a tape recorder, and one-third octave band analysis instrumentation calibrated and operated over a frequency range of 180 to 80,000 Hz. The output is on magnetic tape, which is used to make computer plots of one-third-octave band level versus frequency and other calculations used in the analysis.

3.1.2 Model Description

To simulate the cruise blowing augmentor operating in the takeoff and approach conditions, a new sheet metal nozzle fairing was fitted to a splitter lobe nozzle that was tested in task V (ref. 3). The AAR = 8 corrugated lobe nozzle shown in figures 6 and 7 was selected for these tests. The simulation of the cruise blowing static test configuration was accomplished by installation of the task VII fairing as shown in figure 8. As in the task V program, the nozzle fairing design is established from consideration of airplane structural and duct space requirements and "wind on" test results (ref. 1, section 4.4.2.3, page 30). Utilization of the corrugated lobe nozzles from task V required a deviation in upper fairing
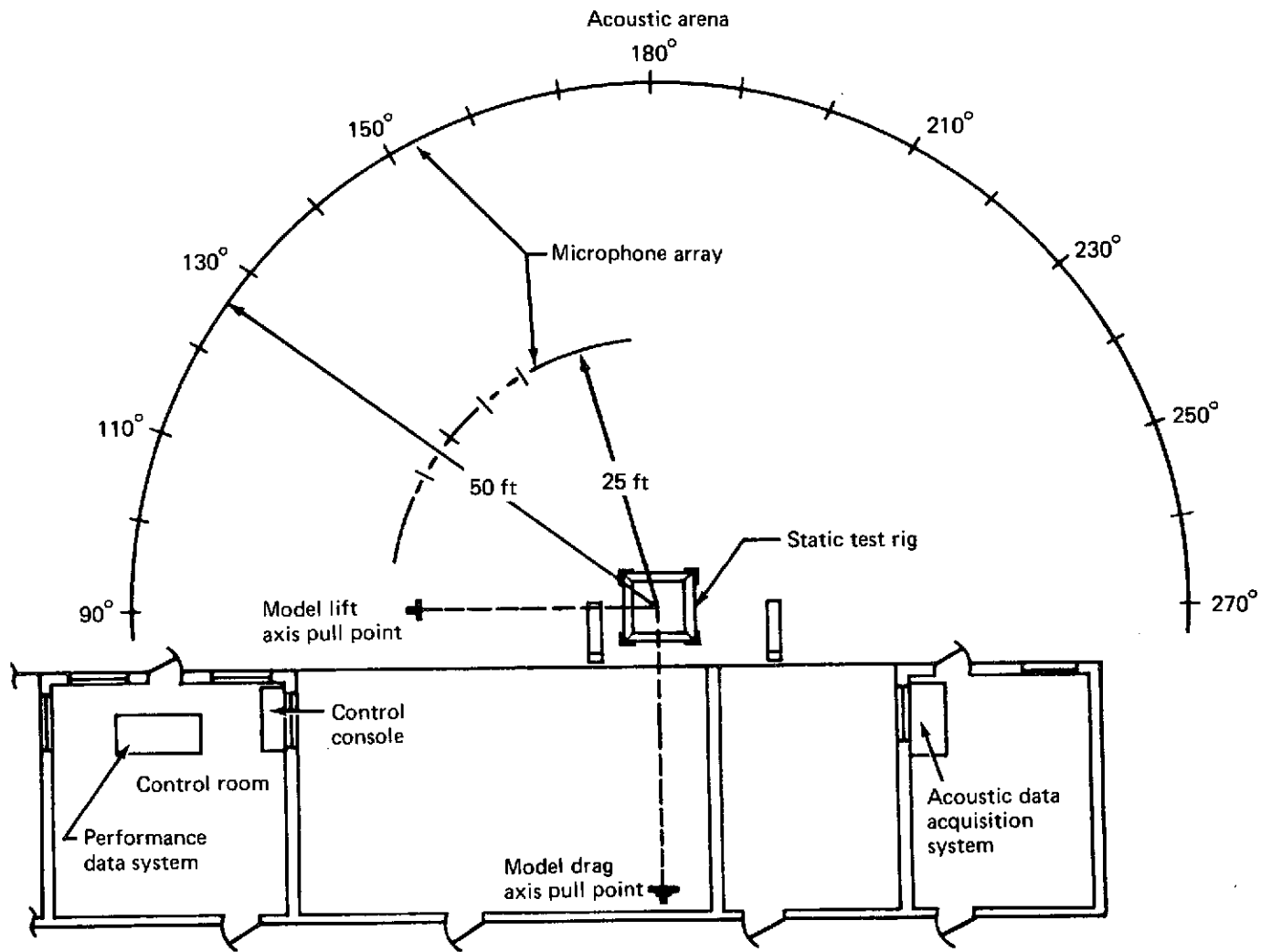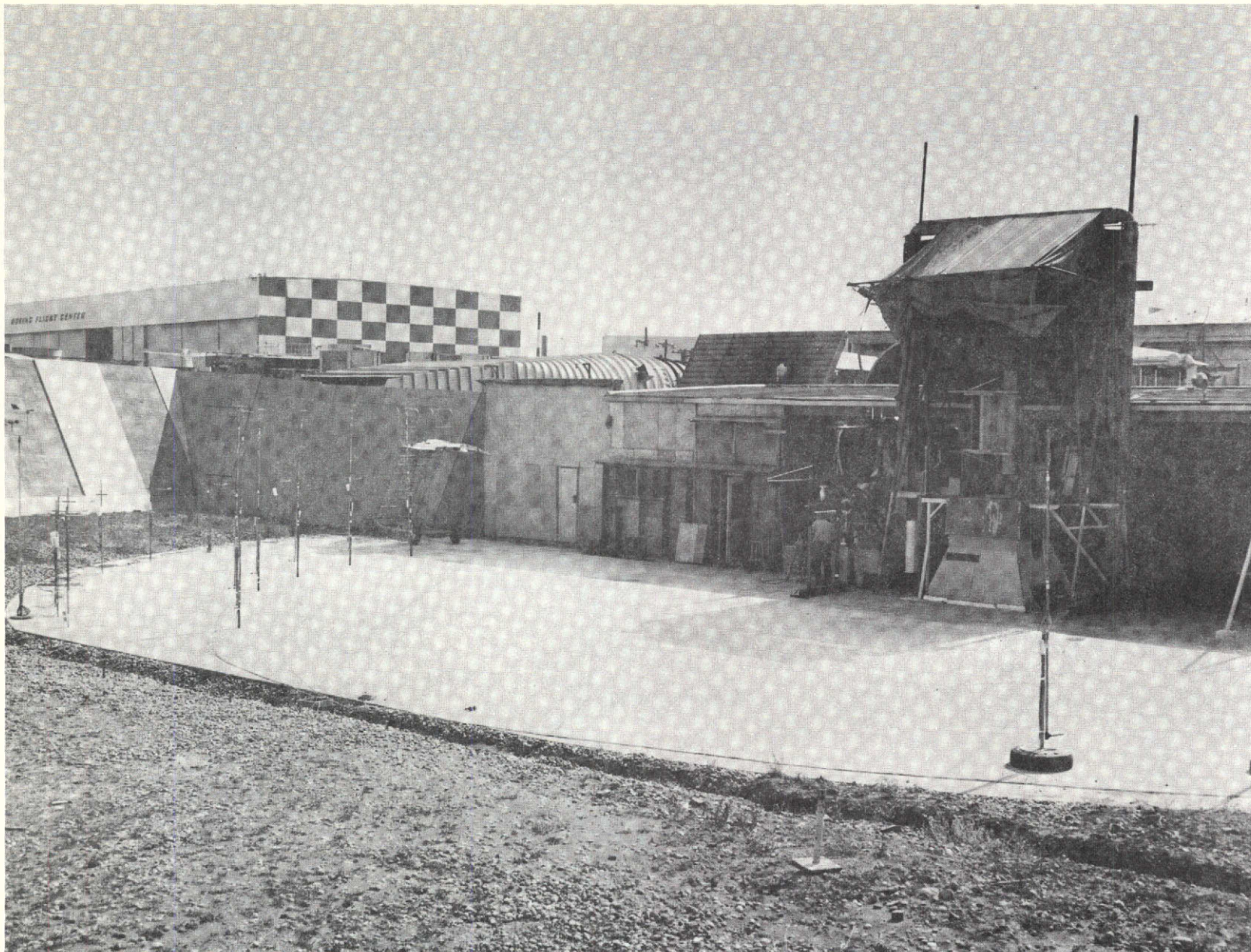
10

FIGURE 4.—STATIC TEST INSTALLATION
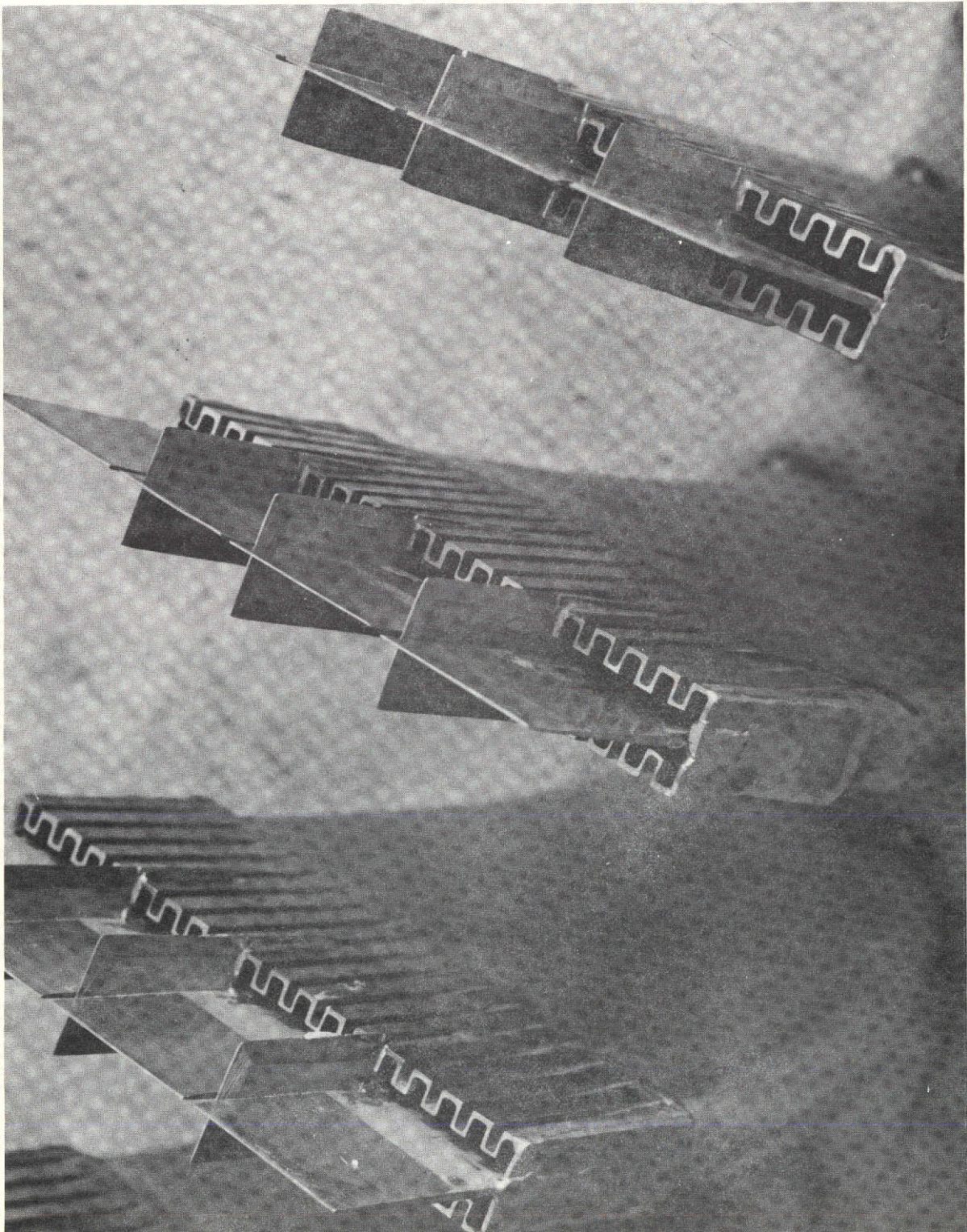
FIGURE 5.—STATIC TEST ARENA

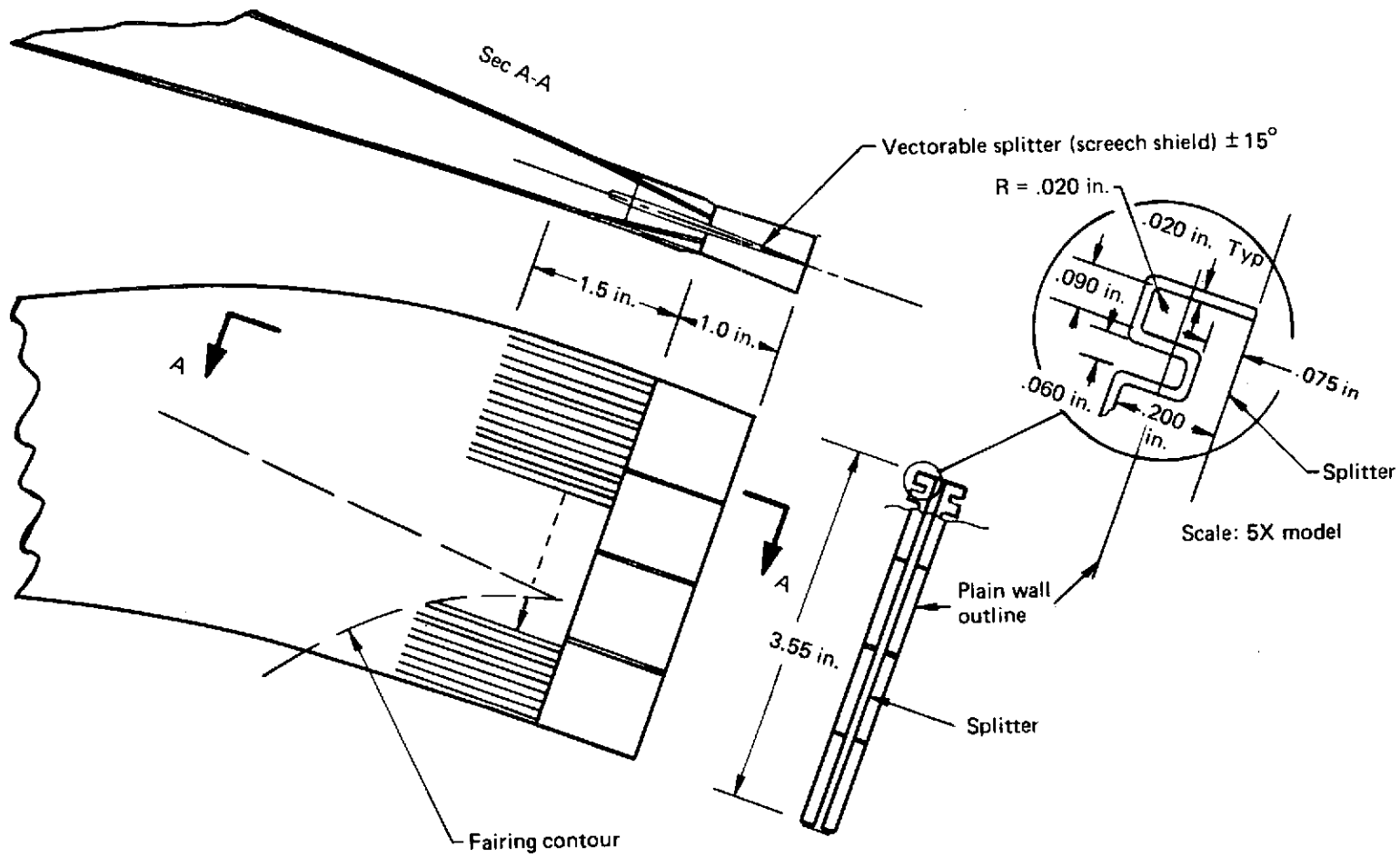FIGURE 6.—SPLITTER LOBE NOZZLE WITH CORRUGATED WALLS, H/P = 1.6, AAR = 8, SHOWING CENTRAL SPLITTER

Sec A-A

Vectorable splitter (screech shield) ± 15°

R = .020 in.

.020 in. Typ

.090 in.

1.5 in.

1.0 in.

.060 in.

.200 in.

.075 in.

A

A

3.55 in.

Plain wall outline

Splitter

Scale: 5X model

Splitter

Fairing contour

FIGURE 7.—SPLITTER LOBE NOZZLE WITH CORRUGATED WALLS, H/P = 1.6

TASK V STATIC TEST CONFIGURATION

Tuned lining

Fairing

Corrugated splitter lobe nozzle
AAR = 8

TASK VII STATIC TEST CONFIGURATION

Fairing

6 in.

19.8 in.

18.5 in.

6 in.
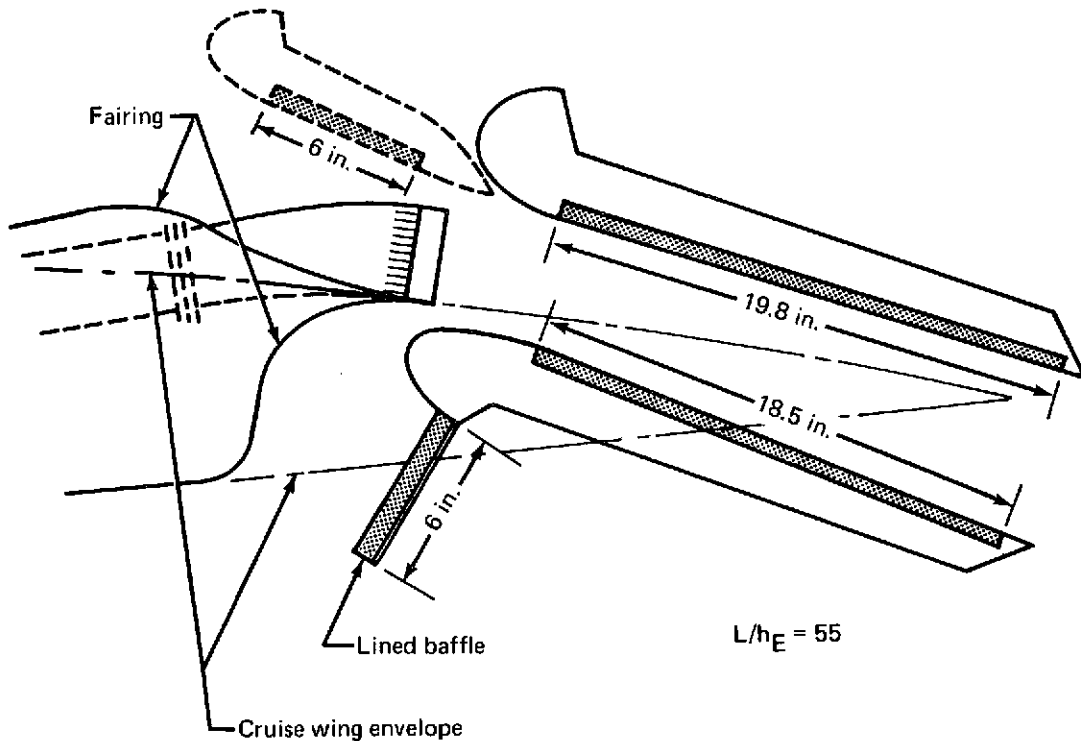
Lined baffle

$L/h_E = 55$

Cruise wing envelope
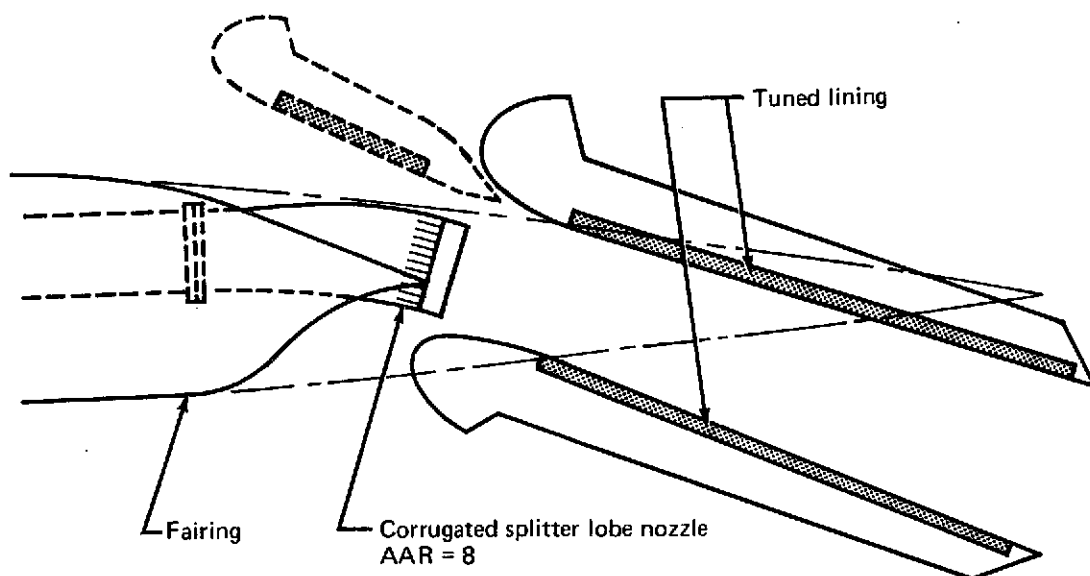
FIGURE 8.—COMPARISON OF TASK V AND TASK VII STATIC TEST CONFIGURATIONS

15

contour. In order to minimize the effects that the nozzle attachment flange might have on secondary air ventilation, the upper fairing was designed to cover this protrusion, and this deviated from the design wing envelope. Any effects on static performance are believed insignificant.

Positioning the lobe nozzles above the wing envelope results in a change in the secondary air flow patterns and potentially has some effect on the augmentor static performance. Augmentor "B" (L/h_E = 55) from task V was used for these tests and tested with and without the task VII multilayer tuned lining (lining IV) (fig. 9).

The basic operating principle of a tuned lining is the conversion of acoustic energy to heat. This is accomplished by placing a suitable dissipator (i.e., the polyimide/glass sheet) at a location of high particle velocity. The location (i.e., distance between the impervious backing sheet and the facing sheet) is determined as a function of the frequencies to be attenuated. The task VII lining is actually two tuned linings combined. One lining consists of the backing sheet, inner cone and the septum, and is tuned for the higher part of the spectrum. The second lining is made up of the backing sheet, the inner and outer core, and the facing sheet; this lining is tuned for a lower frequency than the first lining. The net result is an attenuation over a broad range of the spectrum.

3.1.3 Test Procedures and Performance Definitions

The flap variables are shown in figure 10. The optimization process was conducted with ambient temperature air at two nozzle pressure ratios, with final optimization being made at NPR = 2.6 for δ_T of $0°$, and 1.6 for δ_T of $45°$. Optimization was conducted in the following sequence:

1) ℓ_Z and Z variations were tested with the throat spacing, A_3/A_1, and diffuser angle, θ_D, set at predicted optimums.

2) At optimum ℓ_Z, Z, and θ_D, A_3/A_1 variations were made.

3) At optimum ℓ_Z, Z, and A_3/A_1, a θ_D variation was made.

This procedure was repeated at all flow turning angles investigated. The flow turning angle, δ_T, was varied from $0°$ to $55°$ and optimum thrust augmentation determined for each angle. Because ϕ was measured to be maximum at $\theta_D = 5°$ throughout tasks III and V, the diffuser optimization was not repeated and was set at $5°$ for subsequent testing. Augmentation ratio was hand calculated throughout the optimization process using the uncorrected thrust outputs from the balance. This provided a constant check on the augmentation ratio helping to minimize testing required during the optimization process. The hand-calculated augmentation ratios were normally within 0.02 of the final reduced data. The optimum geometries of augmentor configurations were tested with heated air ($300°$ F) and acoustic and performance data recorded at $0°$, $45°$, $60°$, and $75°$ Beta angles. . Acoustic and performance data were also recorded, using heated air, with the acoustic linings replacing the metal panels (unlined surfaces) on the internal augmentor surfaces. The augmentor model was installed on the static test stand as shown in Fig. 11.
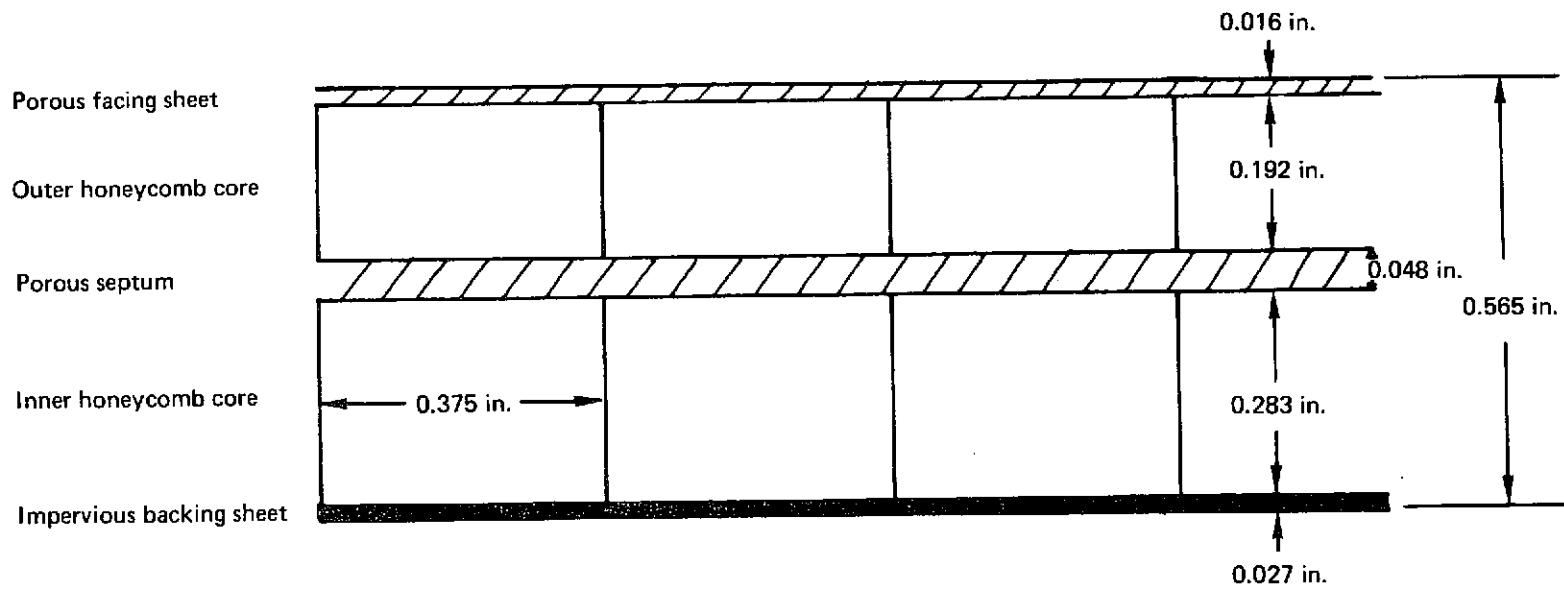
Porous facing sheet

Outer honeycomb core

Porous septum

Inner honeycomb core

Impervious backing sheet

0.016 in.

0.192 in.

0.048 in.

0.283 in.

0.375 in.

0.027 in.
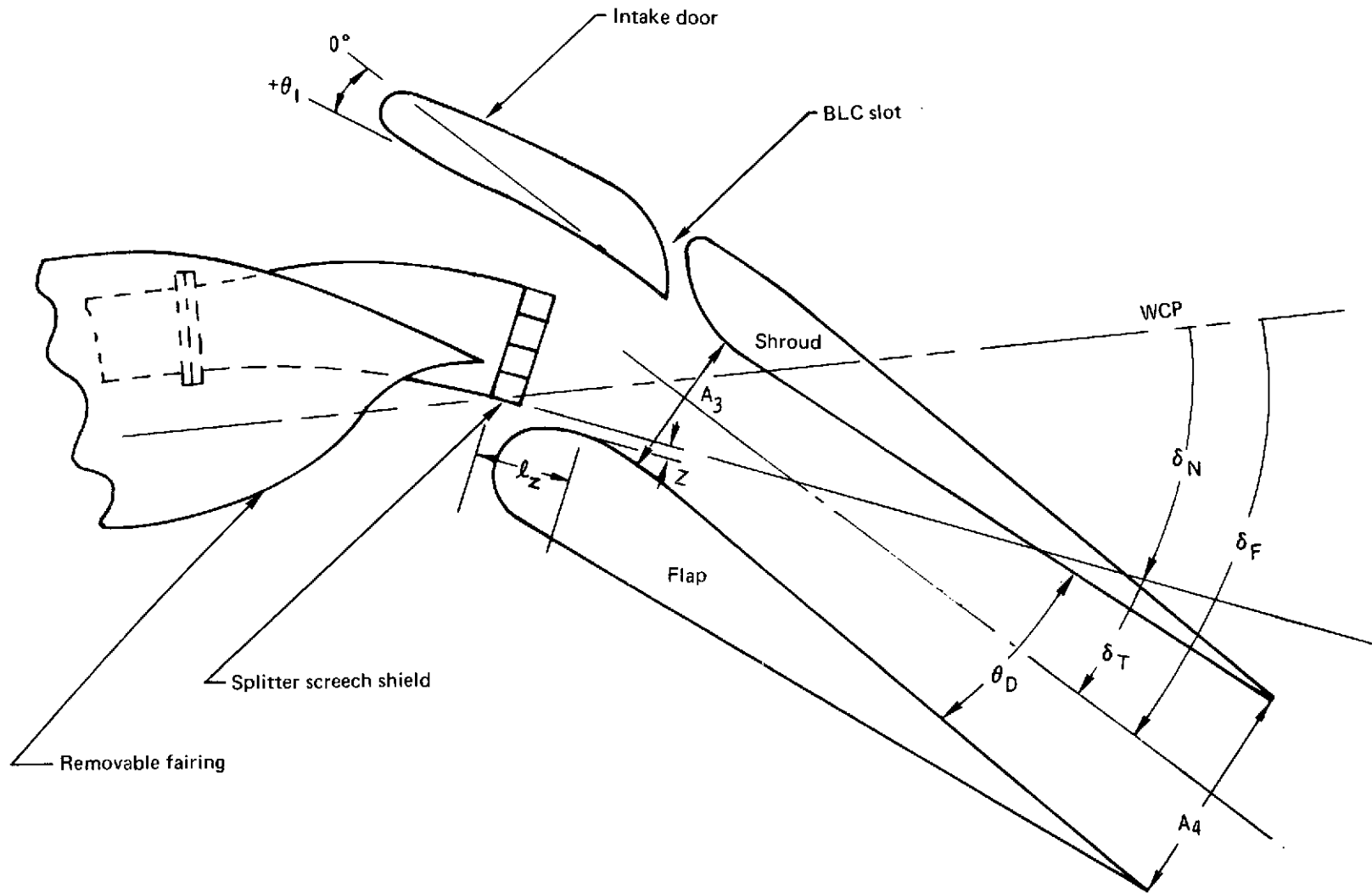
0.565 in.

FIGURE 9.—MULTILAYER TUNED LINING

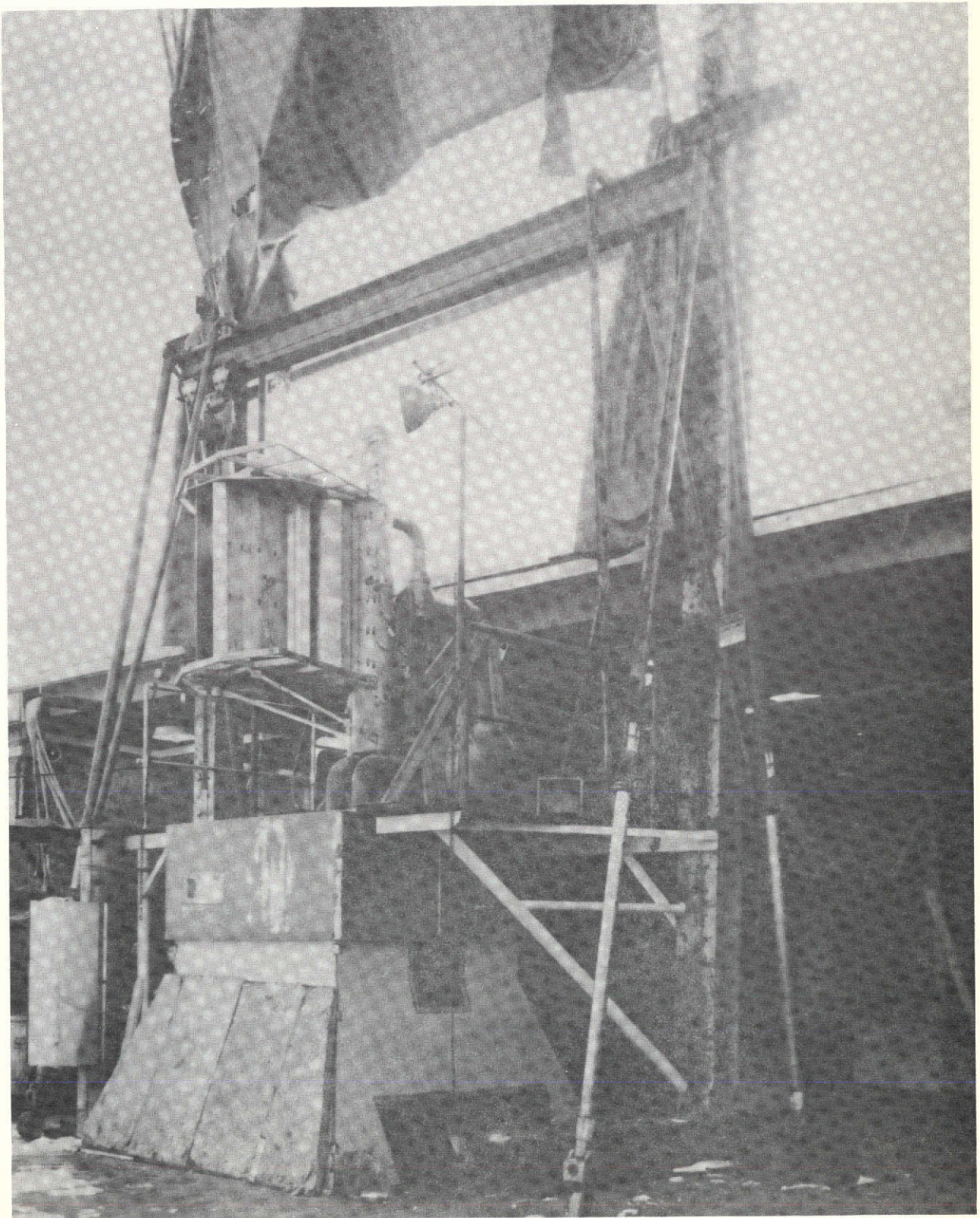FIGURE 10.—AUGMENTOR GENERAL ARRANGEMENT (NO SCALE)

FIGURE 11.—AUGMENTOR SYSTEM INSTALLED ON STATIC TEST STAND

3.1.4 Performance Definitions

The following model thrust performance definitions apply to the performance data presented in this report:

Nozzle Performance

$$\text{Velocity Coefficient, } C_V = \frac{F_N}{mV_I} = \frac{F_N}{C_D m_I V_I}$$

$$\text{Discharge coeffieicent, } C_D = \frac{F_m}{m_I}$$

Augmentor Performance

$$\text{thrust augmentation, } \phi = \frac{F_A}{F_N}$$

where

F_N = measured nozzle thrust, lb_f

m = measured nozzle mass flow, slugs/sec

V_I = isentropic velocity, fps

m_I = ideal mass flow, slugs/sec

F_A = measured augmentor thrust, lb_f

3.1.5 Acoustic Scaling and Extrapolation of Jet Noise

The foundation of acoustic scale-model testing is Lighthill's theory that the total acoustic power radiated from a jet is proportional to the density of the jet, the eighth power of the velocity of the jet, and the second power of a characteristic dimension. To simplify scaling, both the density and jet velocity of the model are identical to the full-scale prototype: only the characteristic dimension is scaled. For a lobed linear array, the characteristic dimension is the lobe width (w). Since w is proportional to the nozzle effective slot height (h_E), scaling is performed using h_E as the characteristic dimension. h_E of the model is 0.43 in., and the average h_E of the selected aircraft configuration is 1.36 in. Thus, the scale factor would be 3.16.

The steps used to scale and extrapolate the jet noise measured from the scale models to a full-scale augmentor wing airplane installation are given in figure 12. In the first step, the acoustic signature is reduced to 27 one-third-octave band sound pressure levels. The spectra are obtained at a number of positions on a 50-ft sphere. These positions are chosen to
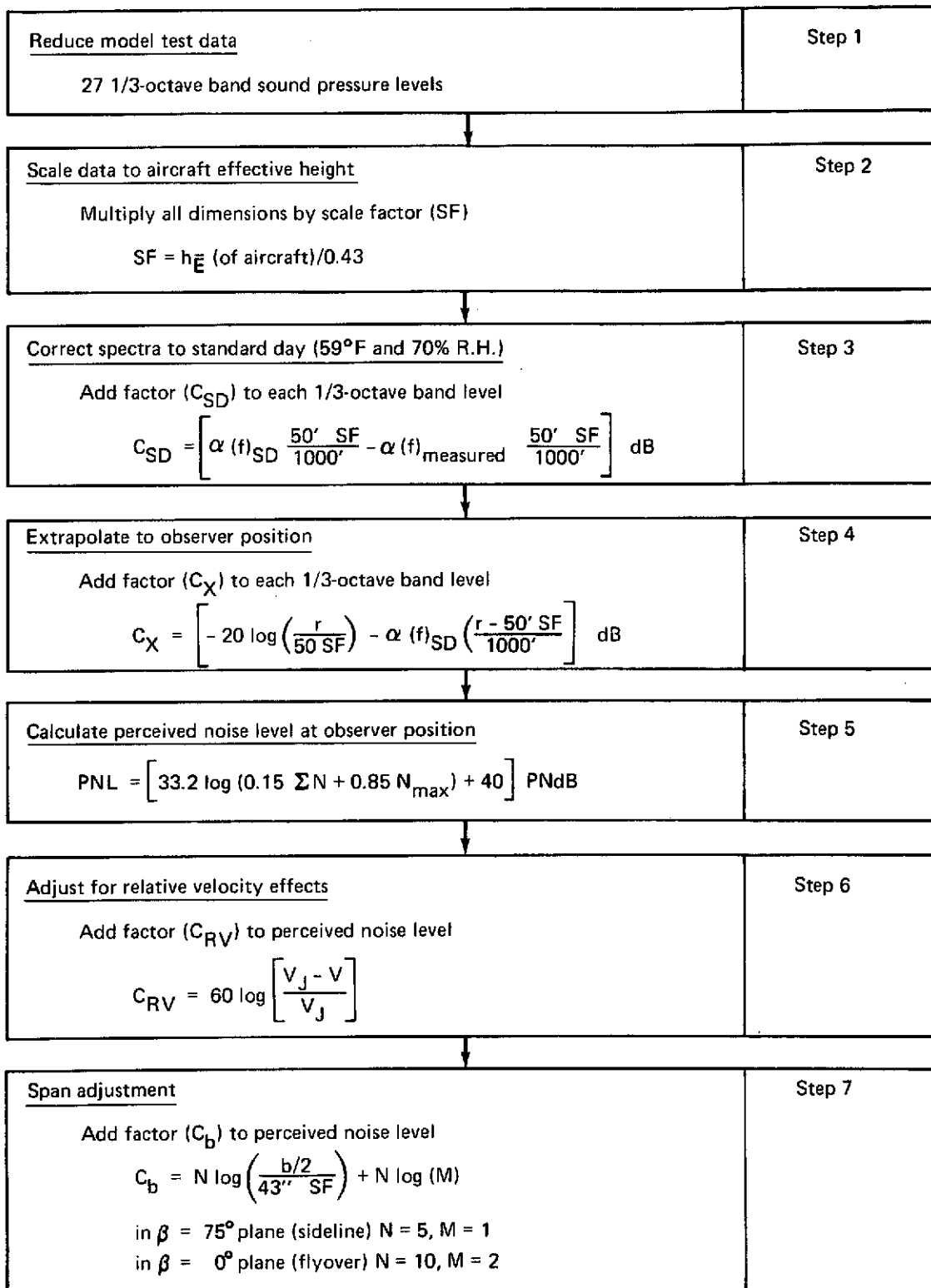
Reduce model test data 27 1/3-octave band sound pressure levels	Step 1

Scale data to aircraft effective height Multiply all dimensions by scale factor (SF) $SF = h_{\bar{E}} \text{ (of aircraft)}/0.43$	Step 2

Correct spectra to standard day (59°F and 70% R.H.) Add factor (C_{SD}) to each 1/3-octave band level $C_{SD} = \left[\alpha\,(f)_{SD}\;\dfrac{50'}{1000'}\;SF - \alpha\,(f)_{measured}\;\dfrac{50'}{1000'}\;SF \right]\,dB$	Step 3

Extrapolate to observer position Add factor (C_X) to each 1/3-octave band level $C_X = \left[-20\,\log\left(\dfrac{r}{50\,SF}\right) - \alpha\,(f)_{SD}\left(\dfrac{r - 50'\,SF}{1000'}\right) \right]\,dB$	Step 4

Calculate perceived noise level at observer position $PNL = \left[33.2\,\log\,(0.15\,\Sigma N + 0.85\,N_{max}) + 40 \right]\,PNdB$	Step 5

Adjust for relative velocity effects Add factor (C_{RV}) to perceived noise level $C_{RV} = 60\,\log\left[\dfrac{V_J - V}{V_J}\right]$	Step 6

Span adjustment Add factor (C_b) to perceived noise level $C_b = N\,\log\left(\dfrac{b/2}{43''\,SF}\right) + N\,\log\,(M)$ in $\beta = 75°$ plane (sideline) $N = 5, M = 1$ in $\beta = 0°$ plane (flyover) $N = 10, M = 2$	Step 7

FIGURE 12.—STEPS USED IN SCALING AND EXTRAPOLATION OF AUGMENTOR NOISE

21

include all probable directions from the airplane to the sideline and flyover observer locations.

Scaling is performed at the second step. It consists of multiplying all linear dimensions by the scale factor (ref. 5). Using a scale factor of 3.16, the 50-ft sphere becomes a 158-ft sphere, the span of the test section becomes 136 in., and the frequency range becomes 50 Hz to 10 kHz.

The spectra are corrected for air absorption to standard day conditions (59° F and 70% RH) (ref. 5). A different correction is required for each frequency band. Ideally this correction would be made as the second step in the procedure; however, in this program it is deferred until after the data are scaled. Since test conditions were close to standard day, errors attributable to this source are estimated to be less than 1 PNdB.

The resulting noise level at the scaled distance is extrapolated to an observer at some other distance in step 4. The inverse square law is applied to all 24 one-third-octave band levels, and an individual correction for air absorption is calculated for each of the band levels. The perceived noise levels is calculated at the observer position in step 5.

A reduction of noise is expected with forward velocity (ref. 7), and it is calculated in step 6. Step 7 is an adjustment for nozzle span. Two cases are shown, one for sideline and the other for flyover. The adjustment consists of two parts. The first takes into account the fact that the model scaled up to the proper h_E is not the correct span (e.g., with a scale factor of 3.16, the span of the scaled model is 136 in., whereas the semispan of the aircraft is 500 in.). The second part takes into account the effect of the other wing. In the flyover case ($\beta = 0°$) the adjustment is equivalent to an area correction. In the sideline case ($\beta = 75°$), shielding is taken into account. The first factor of the adjustment is one-half that of the flyover case, and the second is zero since the fuselage completely shields the other wing (ref. 7).

The observer position with respect to the airplane is illustrated in figure 13. Spherical coordinates are used to define a cone whose axis is the thrust axis of the augmentor system, with the vertex of the cone in the center of the augmentor nozzle exit plane. The axis intersects the ground plane at an angle determined by flight attitude and flap deflection angle.

The three variables that define the observer position are:

1) The distance, r, along the element of the cone passing through the observer position;

2) The cone half-angle, θ, measured from the forward projection of the augmentor thrust axis, and

3) The rotation angle, β, measured about the augmentor thrust axis from the vertical plane (body buttock line (BBL) = 0) beneath the airplane, to the observer position.

22

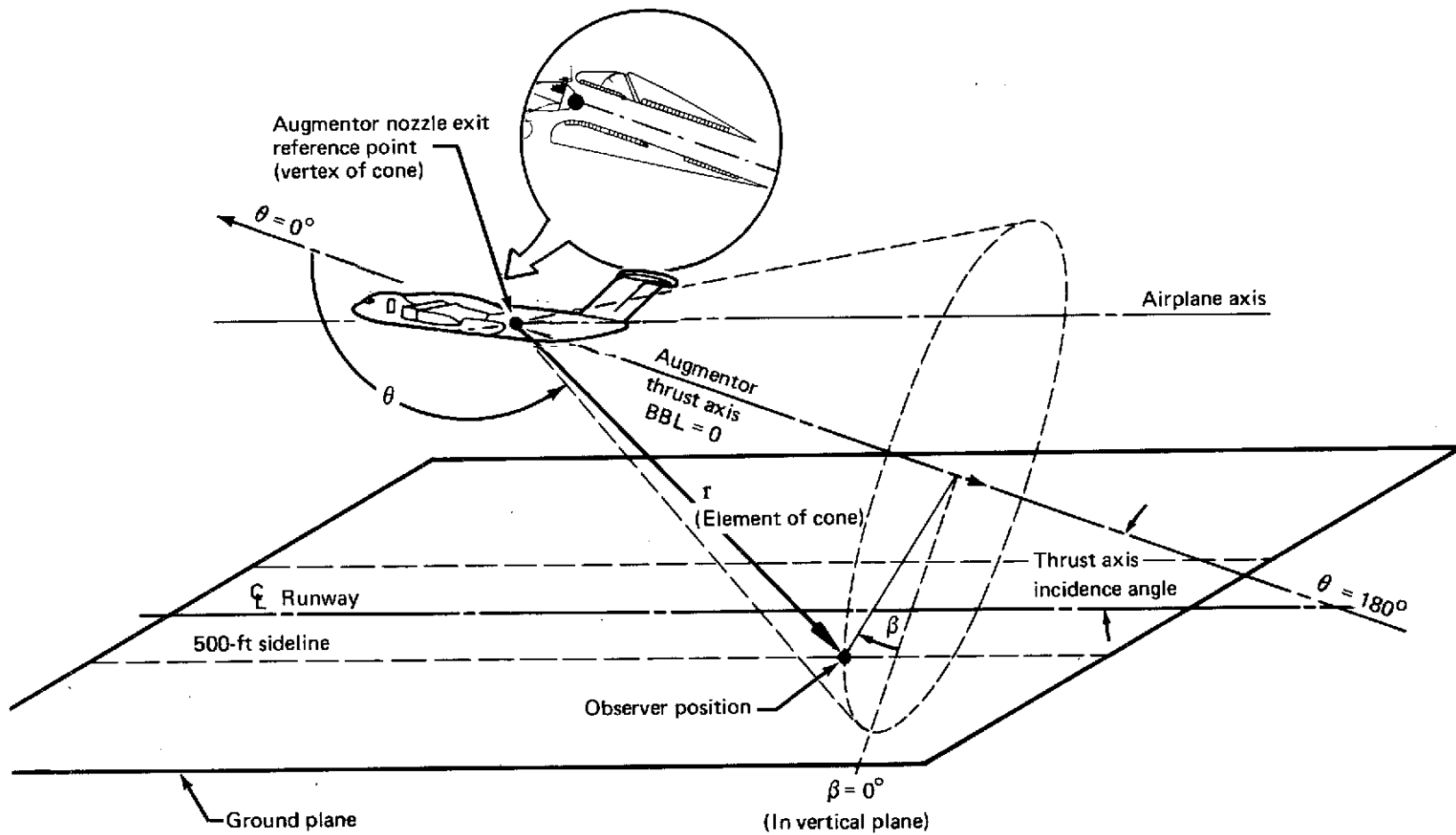FIGURE 13.—COORDINATE SYSTEM TO RELATE OBSERVER POSITION TO AUGMENTOR NOISE SOURCES

The plane defined by $\beta = 90°$ and the augmentor thrust axis is parallel to and lies between the augmentor flap and shroud. The flyover noise is measured in the plane defined by $\beta = 0°$ and the augmentor thrust axis; i.e., the plane defined by BBL = 0.

3.2 RESULTS

All acoustic and performance tests were conducted using the corrugated splitter lobe nozzles and the augmentor "B" flap (ref. 3), shroud and intake. The augmentor was tested with and without a multilayer tuned acoustic lining. By use of interchangeable sheet metal fairings, the cruise blowing augmentor (valveless design) and the task V augmentor (ref. 3) were simulated and tested through augmentor flow turning angles (δ_T) varying from $0°$ to $55°$. The task VII configuration was tested at higher turning angles because of the small precant angle (δ_N) required for cruise performance.

Both task V and task VII configurations were tested for the optimum nozzle positions (ℓ_z and Z) for each turning angle tested. The intake door was installed at turning angles of $45°$ and $55°$ only. The lower baffle was installed for all tests with a lined configuration. The lower baffle was positioned such that lower gap ventilation was not restricted and thrust performance was not affected.
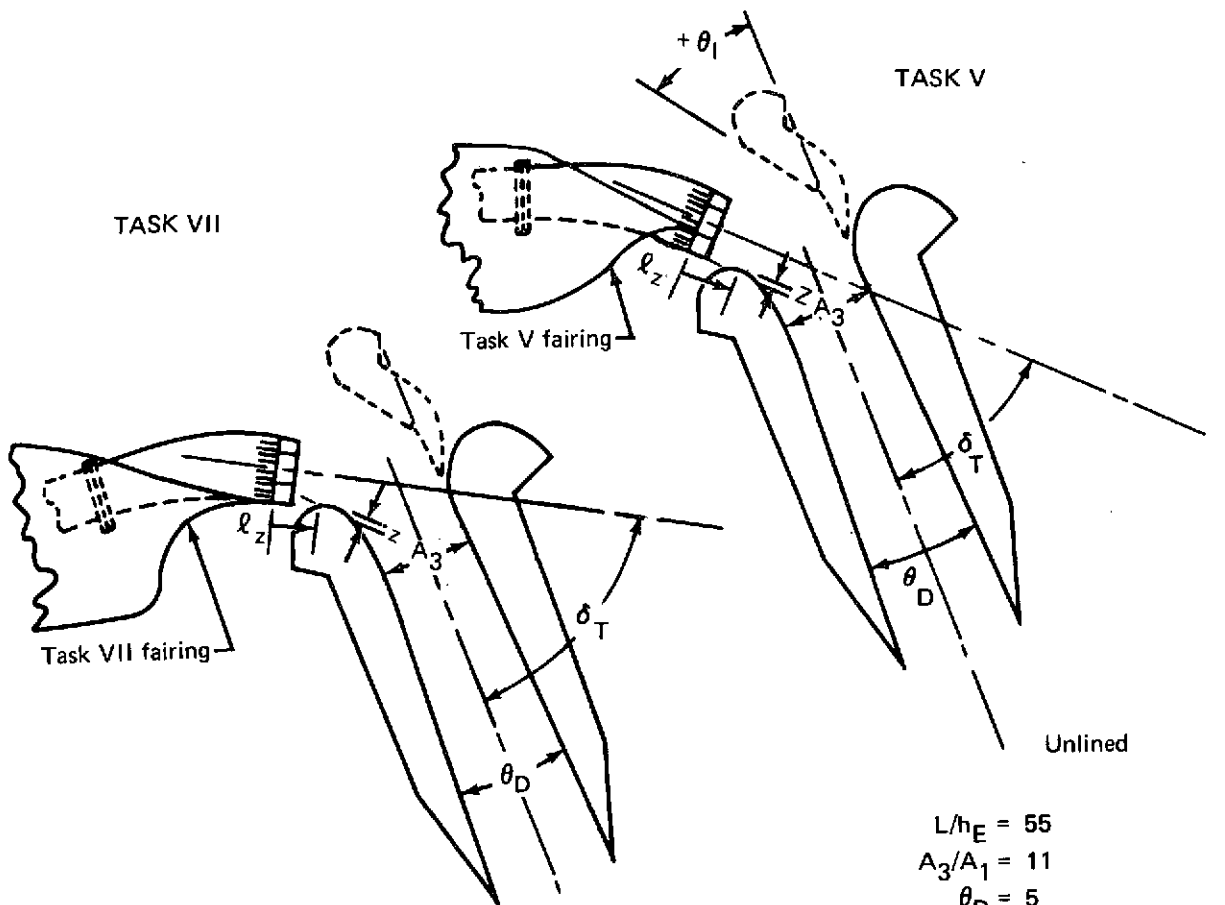
3.2.1 Augmentor Flow Turning Performance

The optimum static thrust configurations (T_{air} = amb) at each flow turning angle tested are shown in figure 14. The task V configuration produced a static thrust augmentation of 1.385 at a turning angle of $0°$. This agreed exactly with the performance measured when the same configuration was tested during task V. The static thrust augmentation dropped to 1.15 at a turning angle of $45°$ (NPR = 1.6).

Installation of the task VII fairing converted the augmentor to a system simulating the cruise blowing (valveless design) configurations. These changes in the relative position of the nozzle, fairing, and flaps result in altering the secondary air ventilation patterns. With the nozzle precant angle (δ_N) limited to values near $10°$ for cruise performance requirements, larger augmentor flow turning angles (δ_T) are required for a given flap deflection (δ_F) when compared with the task V augmentor.

As indicated in figure 14, the cruise blowing augmentor (task VII fairing) produces somewhat lower static thrust augmentation levels than the task V augmentor, particularly at the higher turning angles. The thrust levels are nearly equal at $\delta_T = 0°$ and are about 4 counts different (.04) at $\delta_T = 45°$. At a flow turning angle of $55°$ the task VII augmentor performance fell off to a thrust augmentation slightly over 1.0.

The task VII augmentor entrains most of its secondary air from the upper surface and tends to restrict air from the lower side. The turning performance data indicates that this problem is more severe at high flow turning angles.

24

CORRUGATED SPLITTER LOBE NOZZLE, H/P = 1.6

$L/h_E = 55$
$A_3/A_1 = 11$
$\theta_D = 5$
$\ell_z = Opt^*$
$Z = Opt^*$

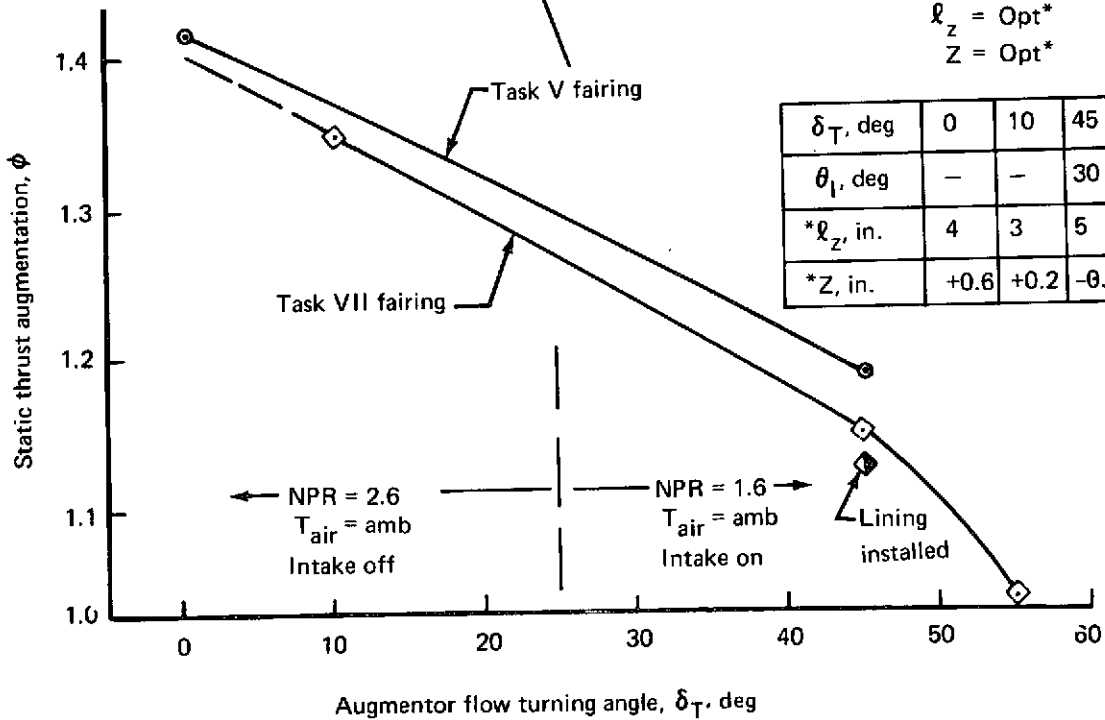| δ_T, deg	0	10	45	55
θ_I, deg	—	—	30	40
$*\ell_z$, in.	4	3	5	5
$*Z$, in.	+0.6	+0.2	-0.4	-0.5

FIGURE 14.—FLOW TURNING PERFORMANCE SUMMARY, TASK V VS TASK VII

3.2.2 Effect of Heated Primary Air on the Lined and Unlined Task VII Augmentor

As in all previous testing, the augmentor is optimized for nozzle position and area ratios with unheated primary air without acoustic lining. With the task VII augmentor set at a flow turning angle of $10°$, the lined and unlined augmentor was tested at three nozzle pressure ratios (2.3, 2.6, and 3.0) with the primary air heated to $300°$ F. As indicated in figure 15, the lining results in a 1- to 2-count loss (.01-.02) in thrust augmentation. The effect of heated primary air is also indicated in figure 15 by comparing the unlined performance levels at a nozzle pressure ratio of 2.6. The thrust augmentation loss due to heated primary air is approximately 4 counts (.04). These thrust augmentation losses due to lining and heated primary air are in close agreement with these effects measured in task V (ref. 3).

The task VII augmentor with tuned lining installed, was also tested with and without heated primary air at a flow turning angle of $45°$. The effect due to heat is again measured at 4 counts (.04) at a nozzle pressure ratio of 1.6, as shown in figure 16.

To determine the limiting turning angle for the task VII augmentor geometry operating under approach nozzle pressure ratios, the turning angle (δ_T) was increased to $55°$ and tested unlined and lined with heated primary air. As indicated in figure 17, the static thrust augmentation drops below 1.0 with heated primary air and a lined augmentor. The effects of heated primary air and lining are generally in agreement with the trends measured and discussed above.

Improvement in static thrust augmentation at these high turning angles using large array area ratio nozzles can be expected by increasing the radius of the flap leading edge.

3.2.3 Acoustics

3.2.3.1 Flow Turning Effects

During this series of tests, two basically different types of configurations were tested. The first was the same configuration tested in task V (ref. 3); the other was a valveless design. From an acoustic viewpoint, the significant difference is that the valveless design requires a $12°$ additional turning of the jet efflux. The additional turning is necessitated by the installation of the wing nozzle on the top of the wing. Small nozzle precant angles must be used to conform to the wing contour. The effect of additional turning can be seen in figure 18. The penalty for $10°$ turning is 2 dB OASPL. Since the increase is fairly uniform over the frequency range, the 2-dB OASPL will translate to 2 PNdB after the data is scaled and extrapolated.

The multilayer lining IV suppresses the additional noise associated with turning. Figure 19 shows that the valveless configuration is slightly lower (1 dB OASPL) than the valved configuration. From these data, it is concluded that the effect upon noise level of flow turning through an angle of $12°$ is negligible.
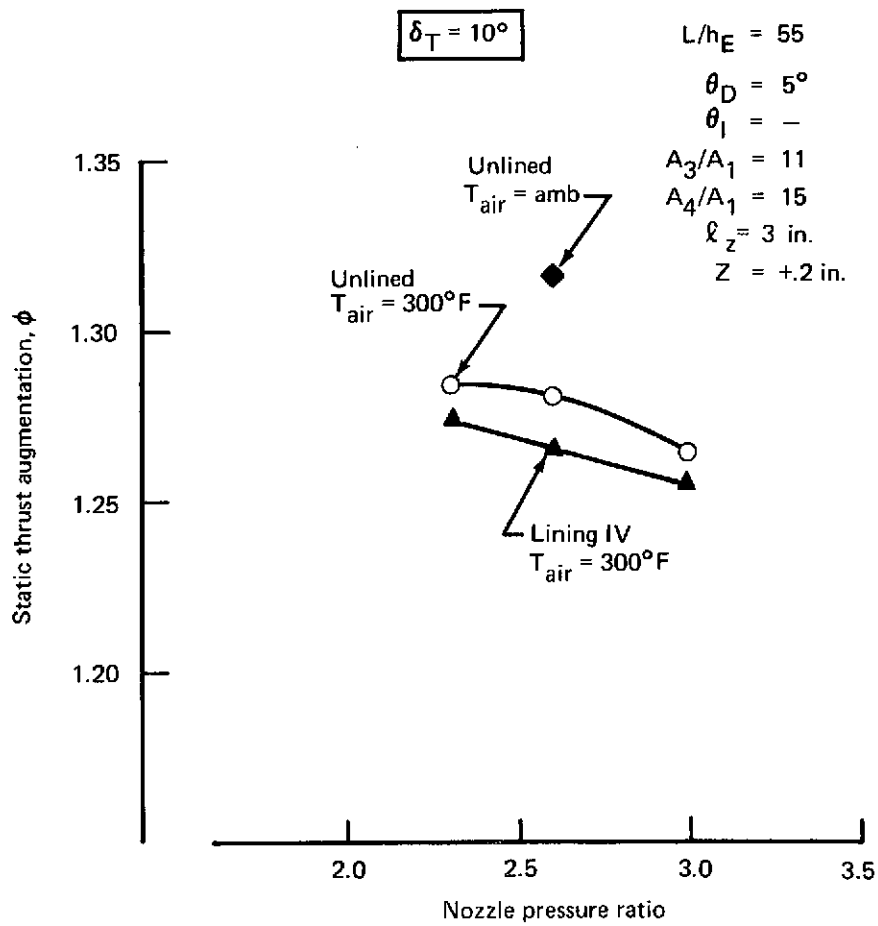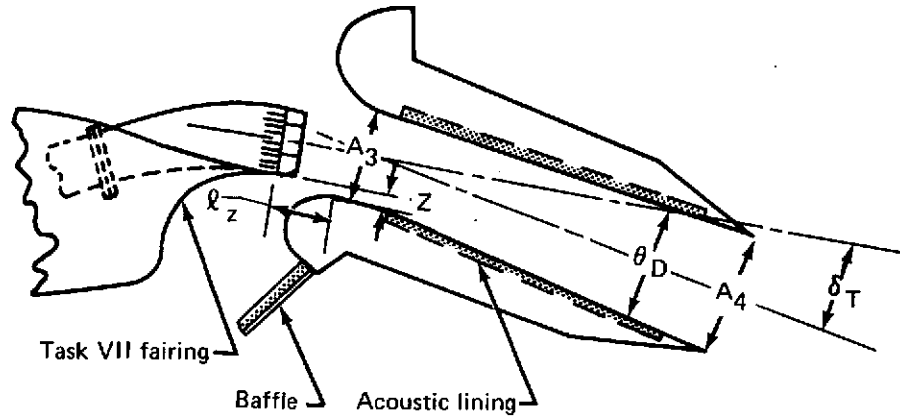
CORRUGATED SPLITTER LOBE NOZZLE, H/P = 1.6

FIGURE 15.—TEMPERATURE AND LINING EFFECTS, 10° TURNING ANGLE

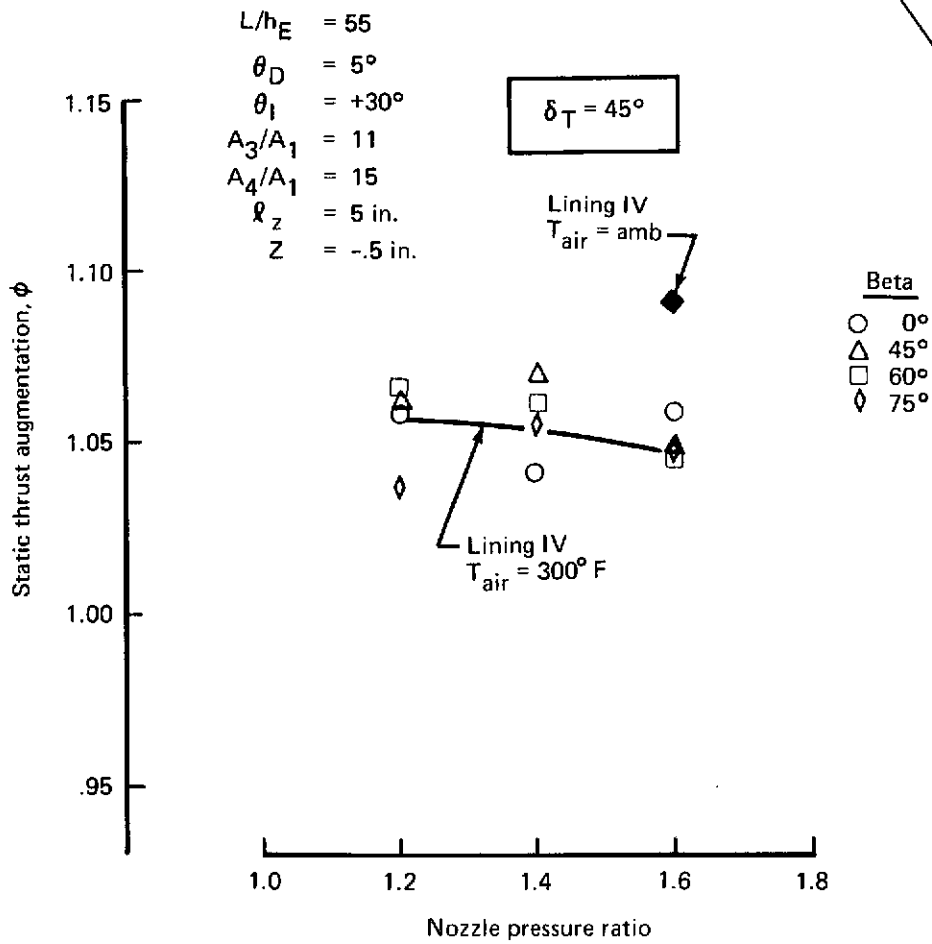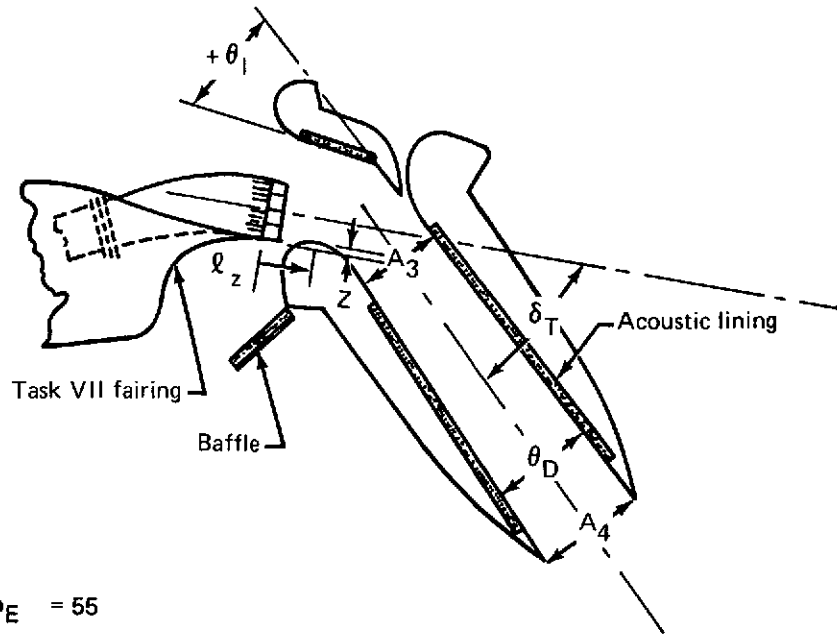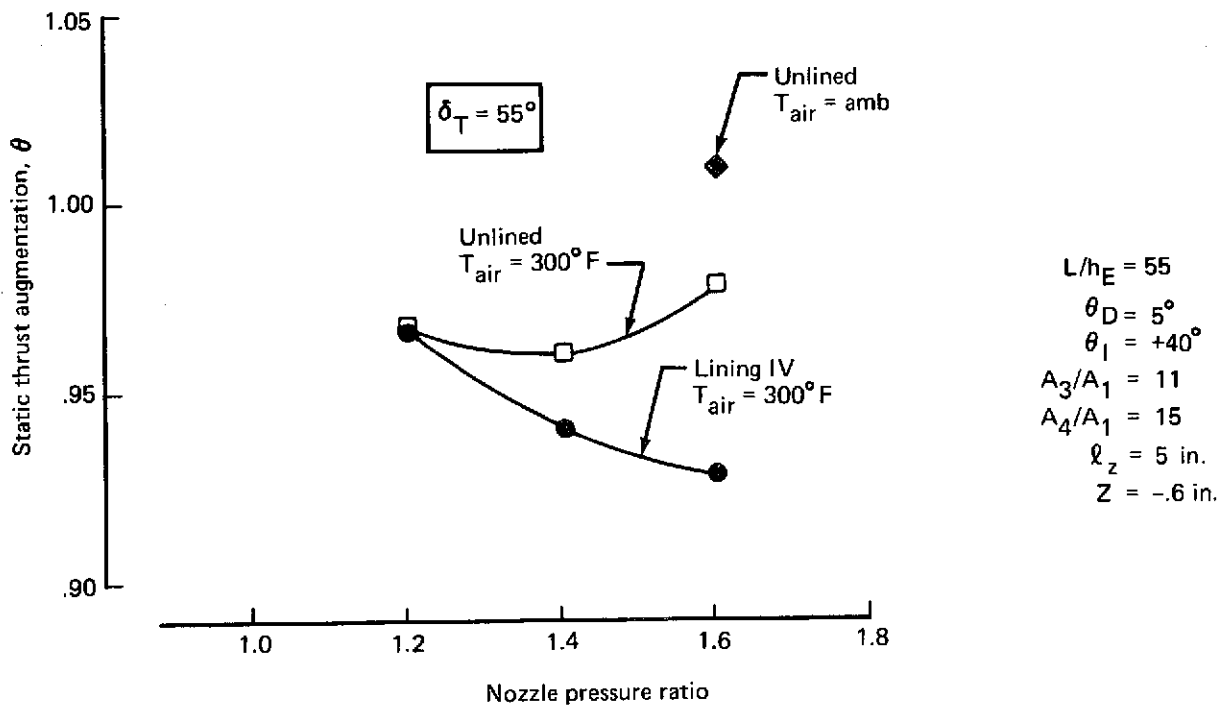CORRUGATED SPLITTER LOBE NOZZLE, H/P = 1.6

L/h_E = 55
θ_D = 5°
θ_I = +30°
A_3/A_1 = 11
A_4/A_1 = 15
ℓ_z = 5 in.
Z = -.5 in.

$\delta_T = 45°$

Lining IV
T_{air} = amb

Lining IV
T_{air} = 300° F

Beta
○ 0°
△ 45°
□ 60°
◊ 75°

Static thrust augmentation, ϕ

Nozzle pressure ratio

FIGURE 16.—TEMPERATURE AND LINING EFFECTS, 45° TURNING ANGLE

28

CORRUGATED SPLITTER LOBE NOZZLE , H/P = 1.6
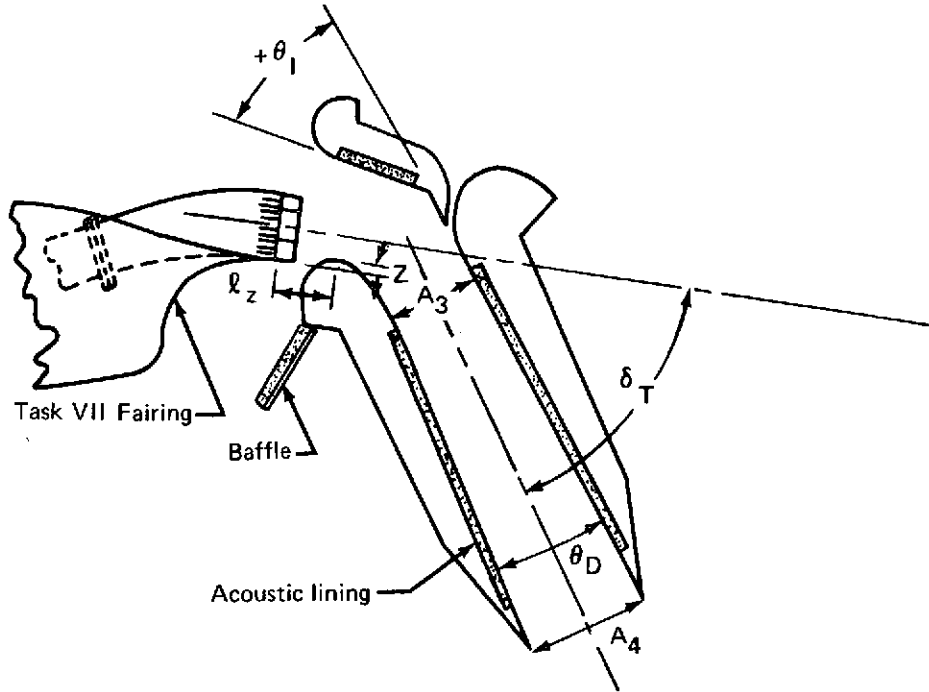
FIGURE 17.—TEMPERATURE AND LINING EFFECTS, 55° TURNING ANGLE

50-FT POLAR ARC SPECTRA—MODEL SCALE DATA
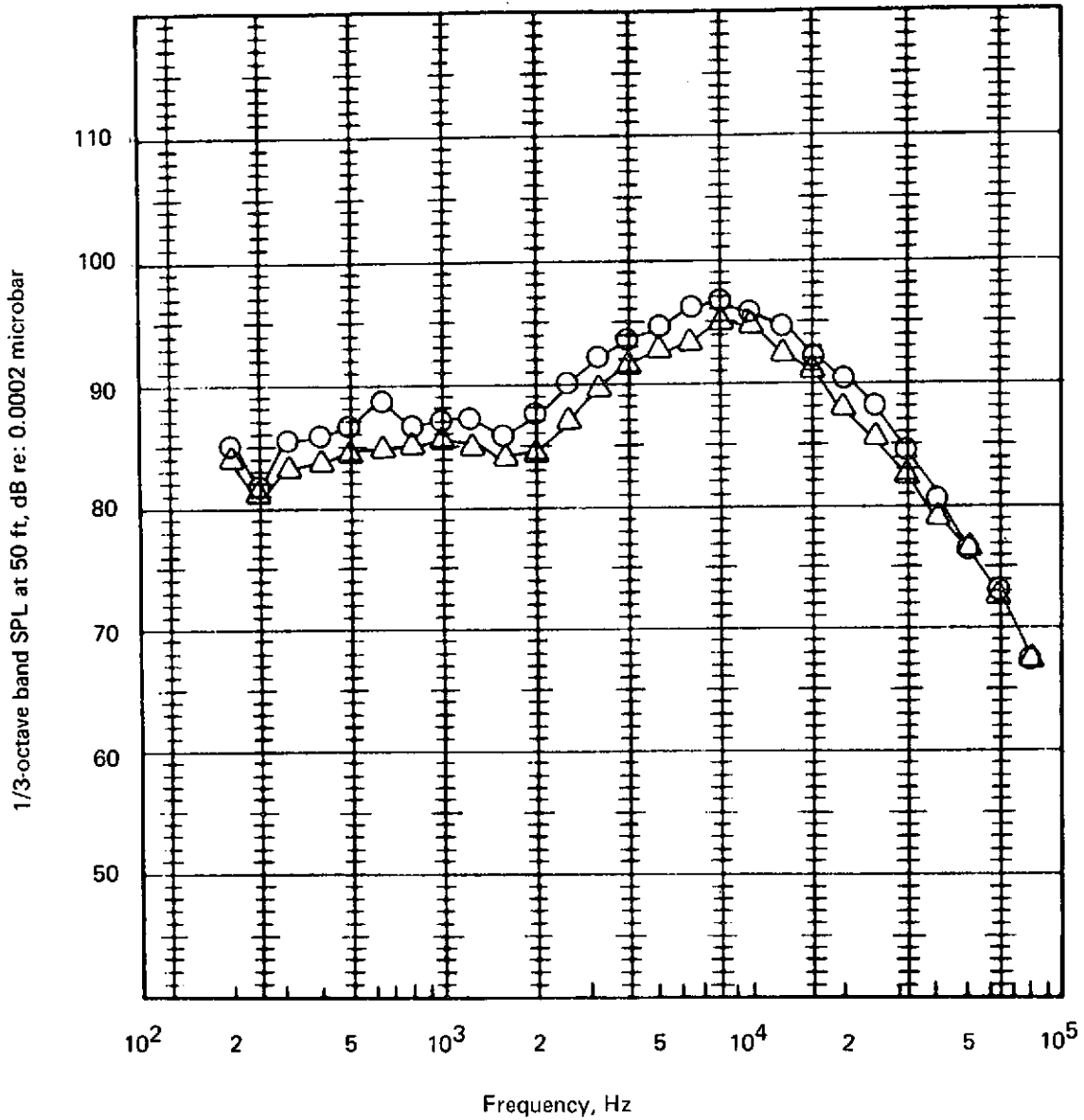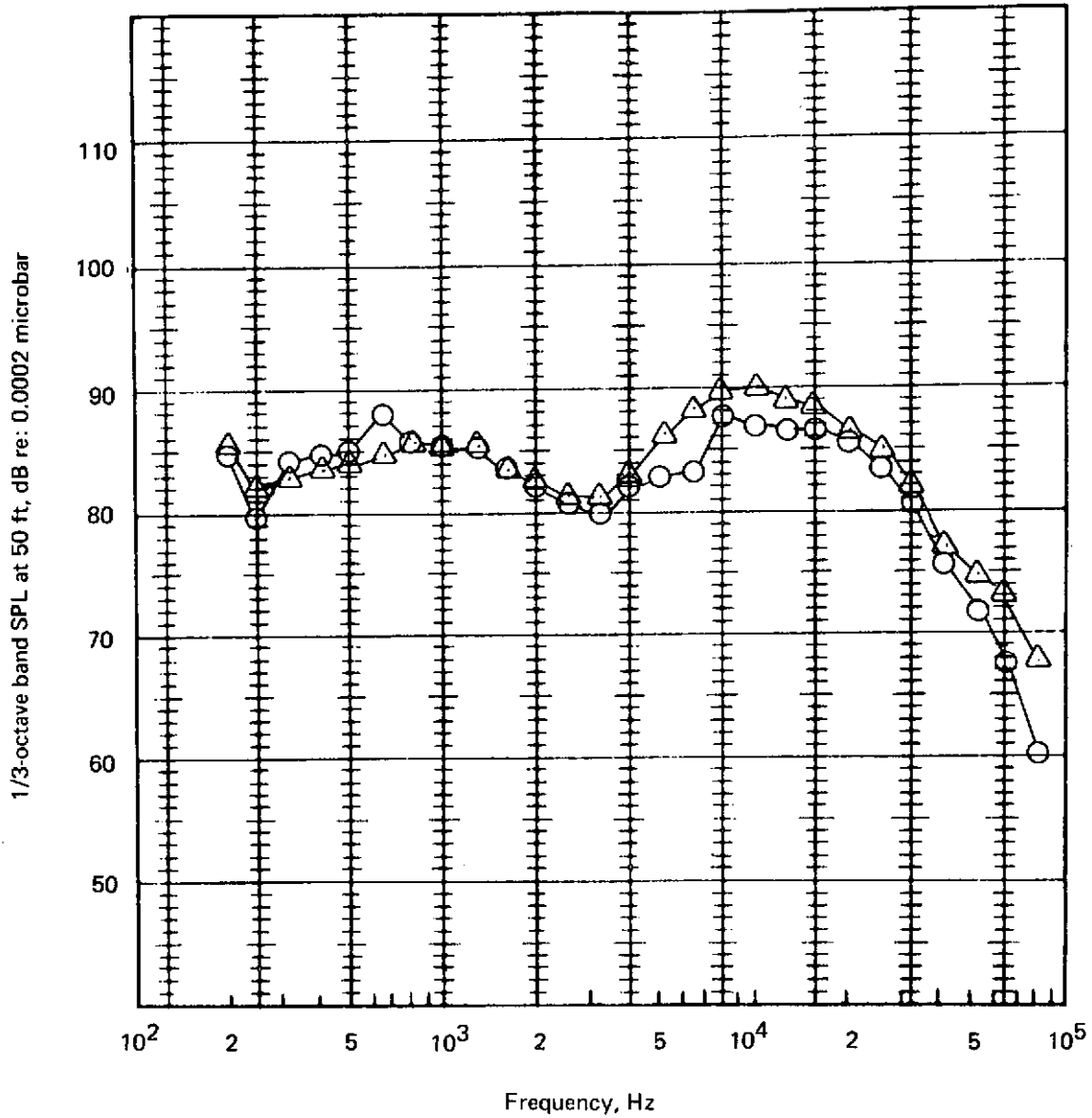
$\bigcirc$ Valveless design $(\delta_t = 10°)$

$\triangle$ Valve design $(\delta_t = 0°)$

20-lobe corrugated nozzle in unlined augmentor

NPR = 2.6, T_T = 300°F, H/P = 1.6, b/h_E = 100, AAR = 8,

L/h_E = 55, β = 75°, θ = 130°

FIGURE 18.—EFFECT OF FLOW TURNING IN UNLINED AUGMENTOR

30

FIGURE 19.—EFFECT OF FLOW TURNING IN LINED AUGMENTOR
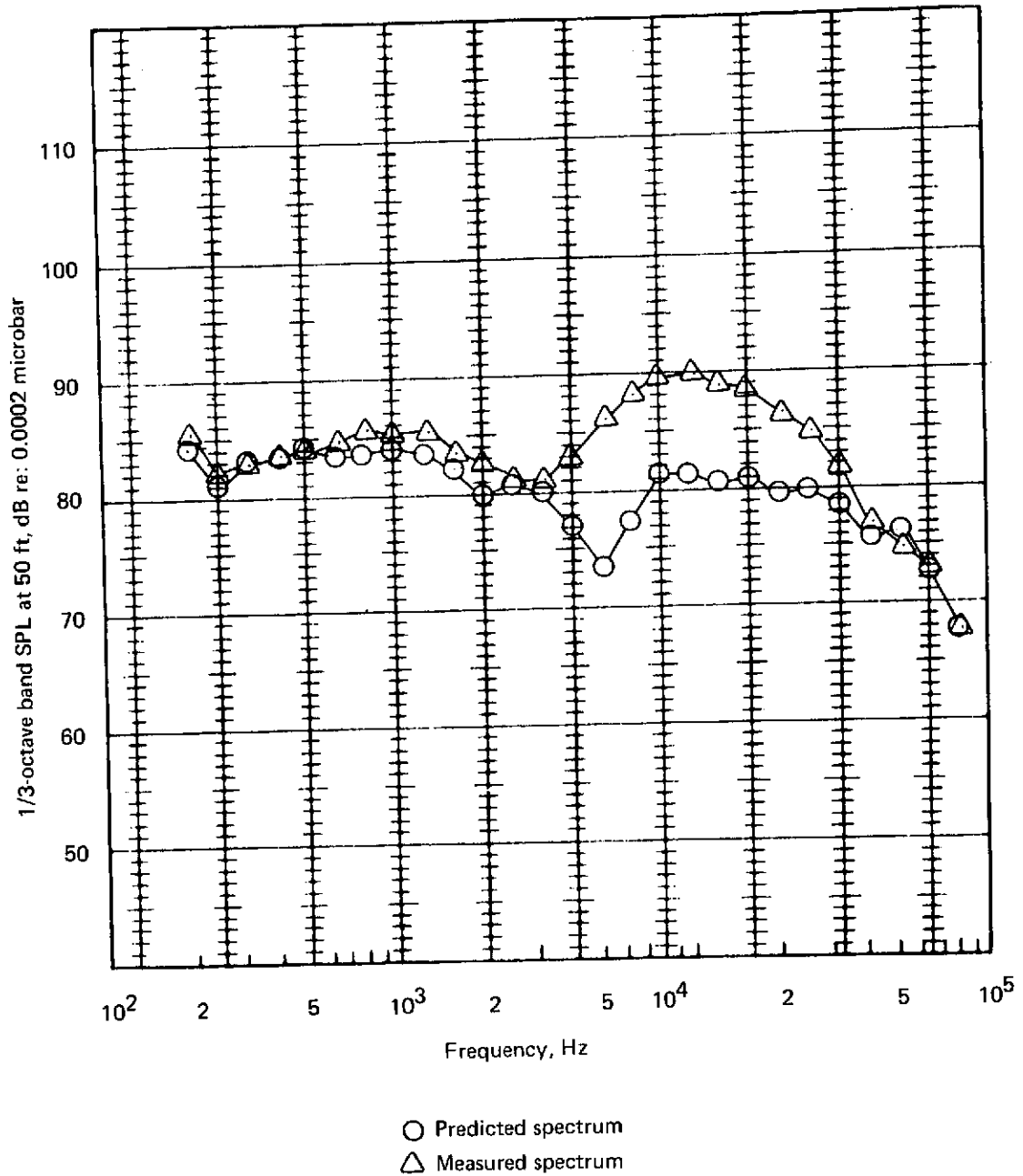
3.2.3.2 Lining Effect

During the previous task (ref. 3) tests were run using the single-row corrugated lobe nozzle and an augmentor with a series of lining sets which were designed for the spectrum of the multirow lobe nozzle. Suppression attributable to the best lining was 4.5 PNdB. A new lining set was designed (lining IV) to attenuate the spectrum of the corrugated nozzle in the augmentor, and a suppression of 7.6 PNdB was predicted. The measured suppression attributable to the new lining was 4.6 PNdB. The predicted and measured spectra are shown in fig. 20. The loss in attenuation at 4 kHz and below was expected and was not used in the prediction for lining IV. The loss in measured PNL suppression is almost entirely caused by the loss in attenuation from 8 to 16 kHz.

The low attenuation in these bands is evidence that the impedance of the outer face sheet is low by a factor of 2 or more. A recheck of the construction of the lining set showed that the measured parameters of the lining were within the design allowable tolerances, and a rerun of the design program gave the same output. The cause of the problem was eventually traced to the inability to measure the impedance of lining material above 6.3 kHz. This measurement is performed with an "impedance tube," and the physical dimension of the tube required to measure above 6.3 kHz becomes smaller than the smallest available microphones. Consequently, impedance values for frequencies above 6.3 kHz are extrapolated from lower frequency impedance data, and the extrapolated data is used in the lining design procedure. This limitation in the prediction procedure would not affect the design of a full-scale lining since attenuation above 6.3 kHz does not materially affect PNL suppression.

3.2.3.3 Directivity Effects

In previous tests (ref. 3), measurements were made in the Beta = $0°$, $30°$, $60°$, and $90°$ planes. Data gathered in the $0°$ Beta plane is used to predict takeoff and approach flyover noise levels. The data from the other three planes is used to predict the takeoff sideline noise levels. The maximum 500-ft sideline level was found consistently in the $60°$ Beta plane for all configurations of nozzles alone or in conjunction with augmentor or flap systems. During the current series of tests, measurements were made in the Beta = $0°$, $45°$, $60°$, and $75°$ planes. When the noise from a nozzle alone is extrapolated to the 500-ft sideline (fig. 21 for example), the maximum noise level is found in the Beta = 60 plane. When the augmentor is added to the suppressor nozzle, either with or without a lining, the maximum noise level is found in the Beta = 75 plane (fig. 22). This effect is due to the suppression of the higher frequencies in the presence of the augmentor. When the higher frequencies are attenuated, the perceived noise becomes dominated by those frequencies generated by the flow downstream of the augmentor. The flow in this region tends to become elliptical or circular in cross section and thus radiates in a more axisymmetric manner. In general, the better the suppression, the closer the peak noise will occur to the Beta = $90°$ plane.

FIGURE 20.—COMPARISON OF PREDICTED AND MEASURED LINING EFFECTS

NPR = 2.6
T_T = 300°F
b/h_E = 100
Data scaled 3.16/1.0

500-ft sideline noise, PNdB

100/1
slot nozzle

Corrugated
lobe nozzle
H/P = 1.6
AAR = 8.0

O — β = 45°
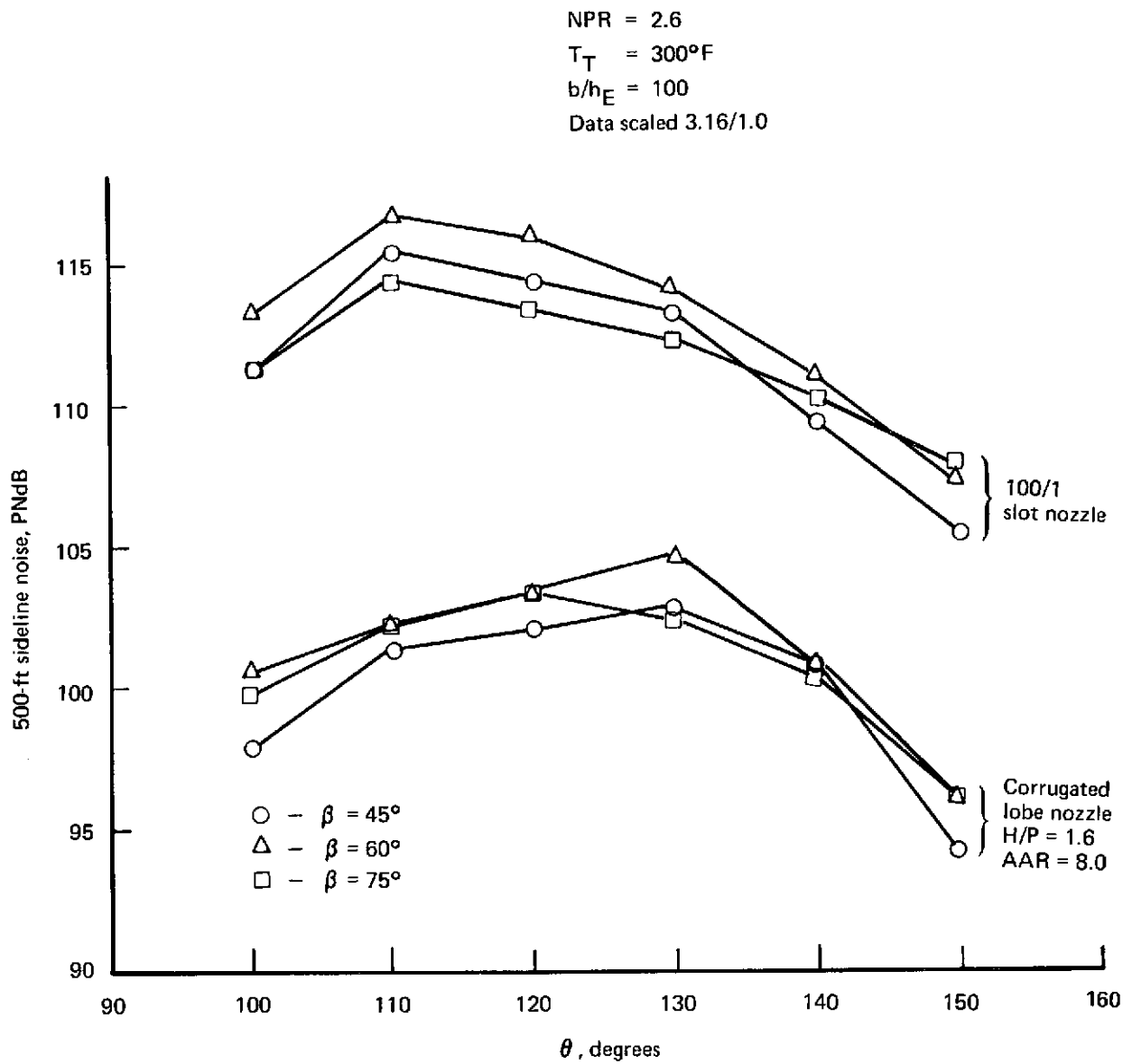△ — β = 60°
□ — β = 75°

θ, degrees

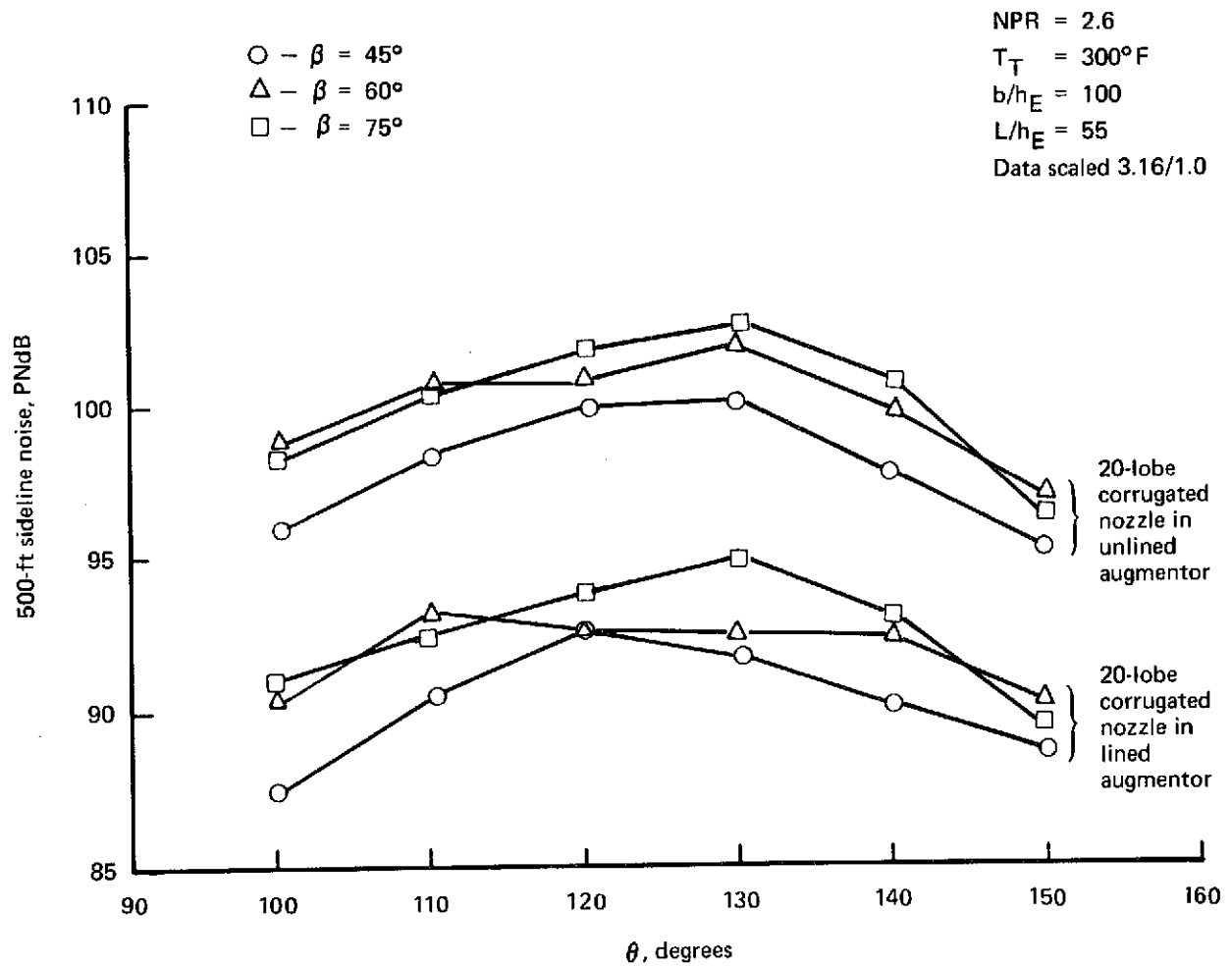FIGURE 21.—DIRECTIVITY OF NOZZLES ALONE

34

FIGURE 22.—DIRECTIVITY OF AUGMENTOR SYSTEMS

4.0 APPLICATION OF TEST DATA TO AIRPLANE DESIGN

Measured scale-model noise levels for the valveless configuration must be scaled and extrapolated to an aircraft. The procedure for 500-ft sideline maximum follows. The 500-ft sideline maximum perceived noise level (PNL_M) as a function of average equivalent slot height (h_E) is shown in figure 23. Curve "A" is test data scaled and extrapolated to the sideline with a Delta of -3 PNdB taken for relative velocity. The slope of this curve is attributable to the change in nozzle area alone; spectrum shape has little effect through this somewhat limited range of h_E. (Spectrum shift is less than one octave band.) By projecting the data into the near future, curve "B" is produced. The Delta from curve "A" to "B" is -5 PNdB. This Delta is comprised of two parts: -3 PNdB for improved linings with optimum tuning and -2 PNdB for full-scale lining effects. In going to a similar nozzle with array area ratio (AAR) of 6 instead of 8, an additional Delta of -2 PNdB may be obtained, producing curve "C". It must be remembered that as h_E increases in this figure, the absolute values of area (A^*), nozzle span (b), lobe width (w), and flap length (L) also increase. Therefore, this data must be modified for prediction of aircraft noise levels.

If an aircraft configuration of a fixed-wing aspect ratio ($\mathcal{R}$) is selected, then the only remaining variable, assuming a fixed fan pressure ratio (FPR), is wing duct pressure loss ($\Delta P/P_t$). Figure 24 shows the relationship between h_E and $\Delta P/P_t$ for an $\mathcal{R}$ of 8.0. Curve "D" is derived from curve "C" of figure 23 by adding the additional acoustic energy from the fixed-length wing nozzle span of 520 in. (ref. 4). An additional correction is required for a fixed flap length. Two such flap lengths are shown for flap chord lengths of 26% and 28% of wing chord, figure 24. It can be seen that a 2% increase of flap chord length is worth 1 PNdB. The highest noise level for a wing aspect ratio 8.0 is 89 PNdB for a 12% duct loss and a 26% flap chord length and array area ratio of 6; for AAR = 8 the highest noise level is 91 PNdB.

This procedure is repeated for a wing aspect ratio 7.5 configuration in figure 25. This $\mathcal{R}$ is perhaps more realistic. From this set of curves, it is found that to meet a 90-PNdB sideline objective a duct pressure loss of less than 10% is required for the 28% flap chord length. For the former case h_E = 1.36 in., the lobe width is 0.85 in. The nozzle span is 500 in., and the flap length is 62 in. The peak sideline spectrum is shown in figure 26 for this case.

36

DATA BASE: RUN 2083

Corrugated lobe nozzle

$w/h_E = 1/(H/P)$

NPR = 2.6

H/P = 1.6

$T_T = 760°R$

Lined augmentor

$L/h_E = 55$
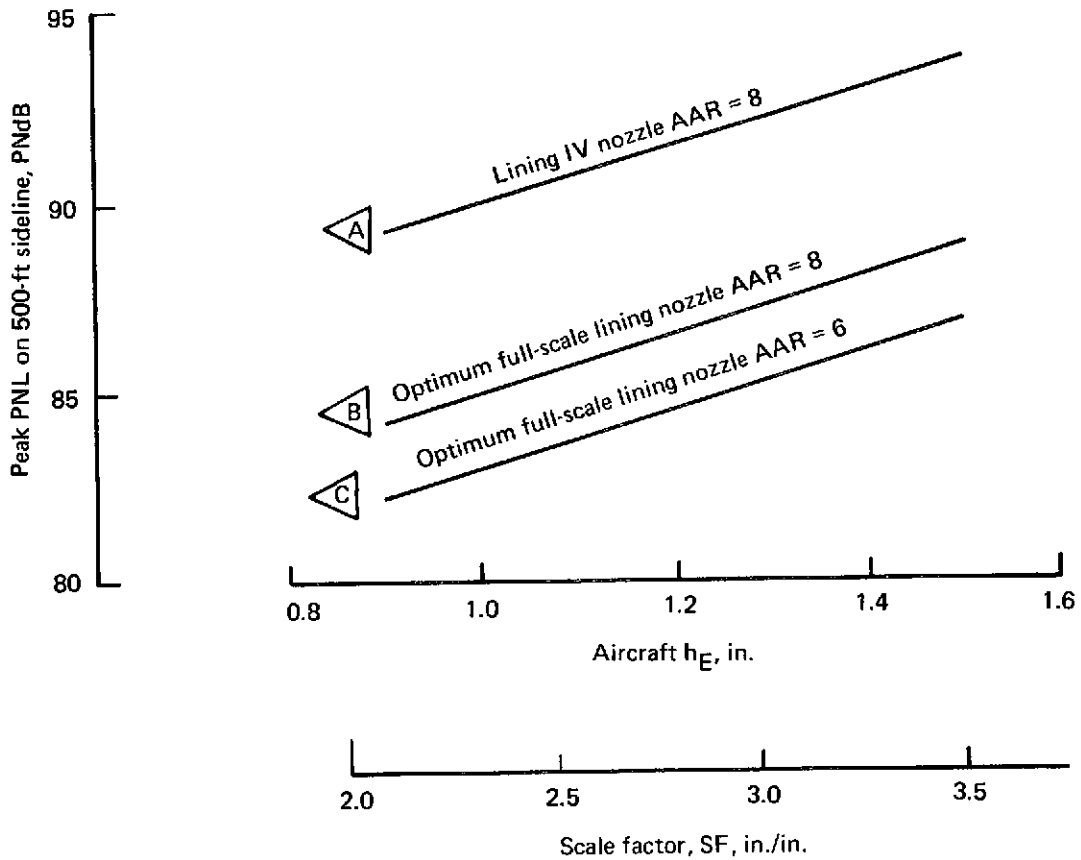
$b/h_E = 100$

Aircraft velocity

$V_A = 80$ ktas

FIGURE 23.—500-FT SIDELINE MAXIMUM AUGMENTOR
NOISE LEVELS INDEPENDENT OF AIRCRAFT CONFIGURATION

DATA BASE: RUN 2083
Corrugated lobe nozzle

$w/h_E = 1/(H/P)$

NPR = 2.6

H/P = 1.6   AAR = 6

T_T = 760°R

Lined augmentor

$L/h_E = 55$ Aircraft velocity

$b/h_E = 100$ V_A = 80 ktas

b/2 = 520 in., L = 56 in. (.26C)
b/2 = 520 in., L = 60 in. (.28C)
b/2 = 520 in., L = 55 h_E

From fig. 23

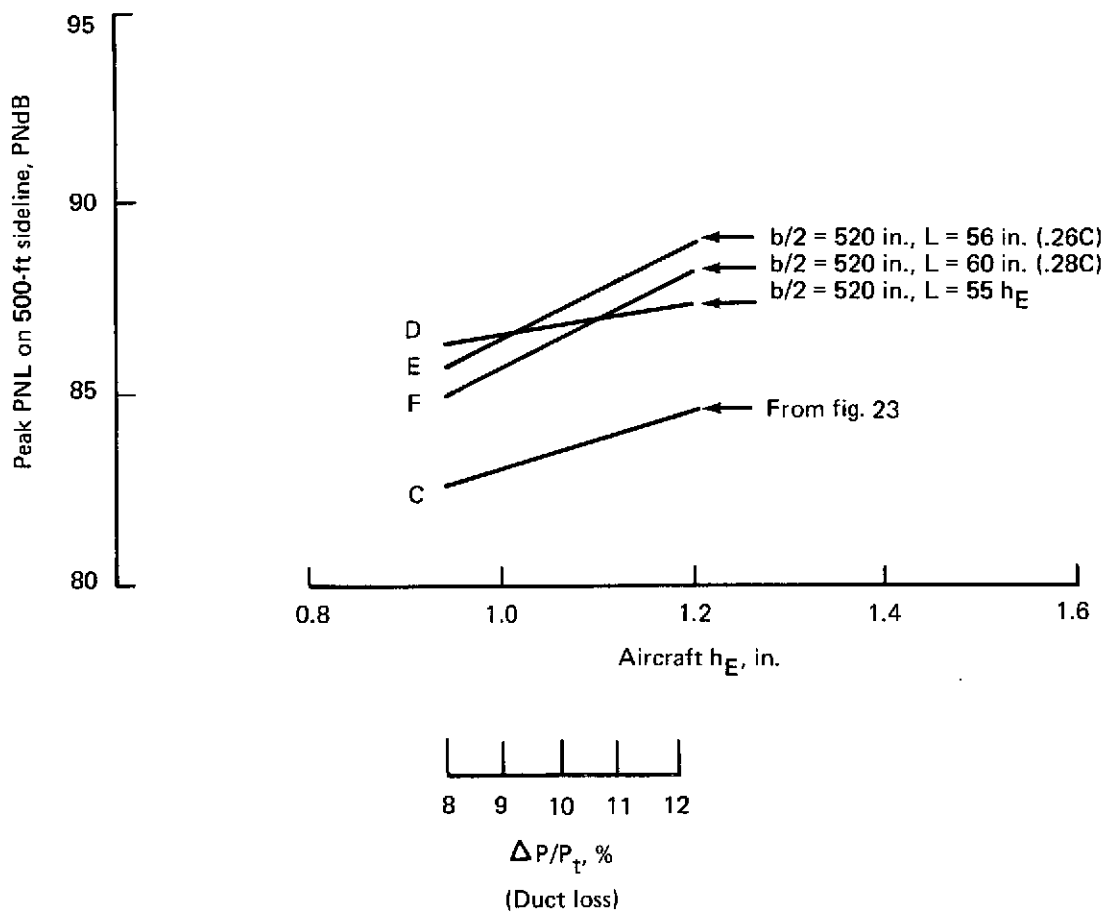$\Delta P/P_t$, %

(Duct loss)

*FIGURE 24.—500-FT SIDELINE MAXIMUM AUGMENTOR NOISE LEVELS
FOR AN AIRCRAFT WITH WING ASPECT RATIO = 7.5*

38

DATA BASE: RUN 2083

Corrugated lobe nozzle
w/h_E = 1/(H/P)
NPR = 2.6
H/P = 1.6   AAR = 6
T_T = 760°R
Lined augmentor
L/h_E = 55   Aircraft velocity
b/h_E = 100 V_A = 80 ktas

b/2 = 500 in., L = 58 in. (.26C) →
b/2 = 500 in., L = 62 in. (.28C) →
b/2 = 500 in., L = 55 in. h_E

From fig. 23 →

Peak PNL on 500-ft sideline, PNdB

Aircraft h_E, in.
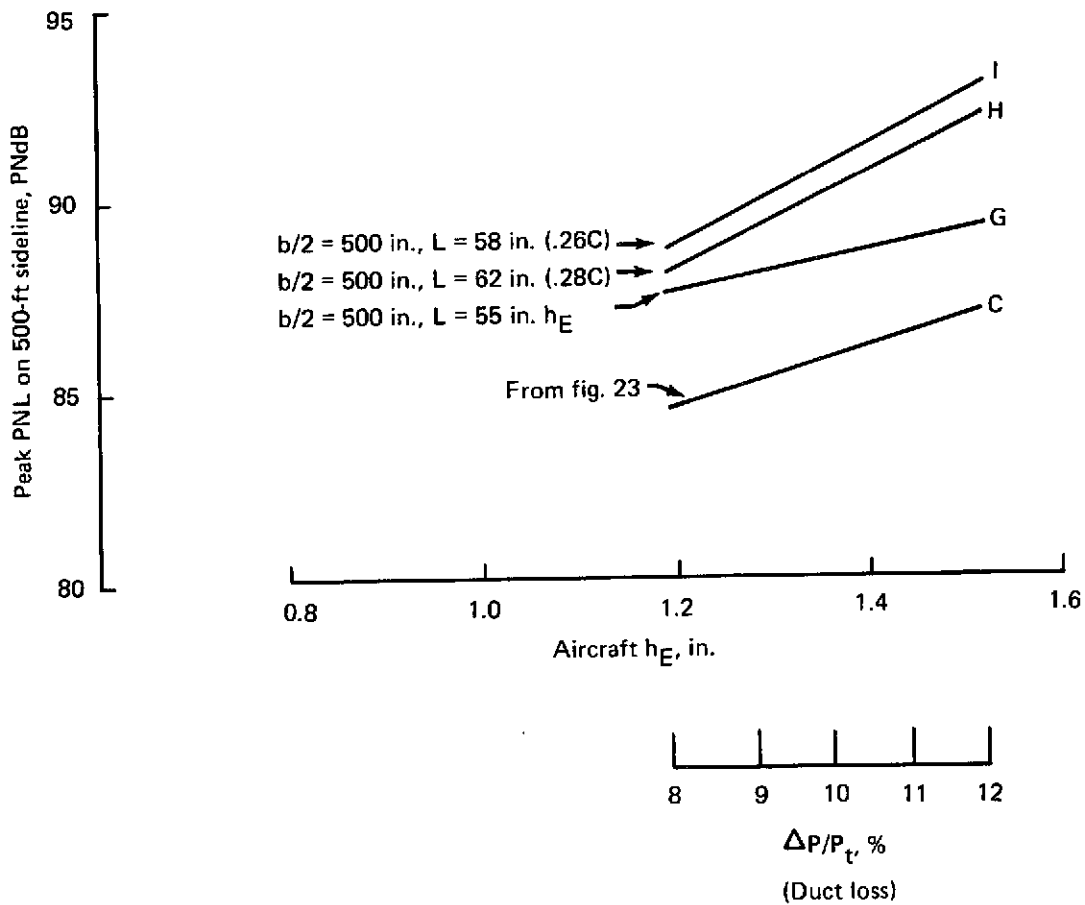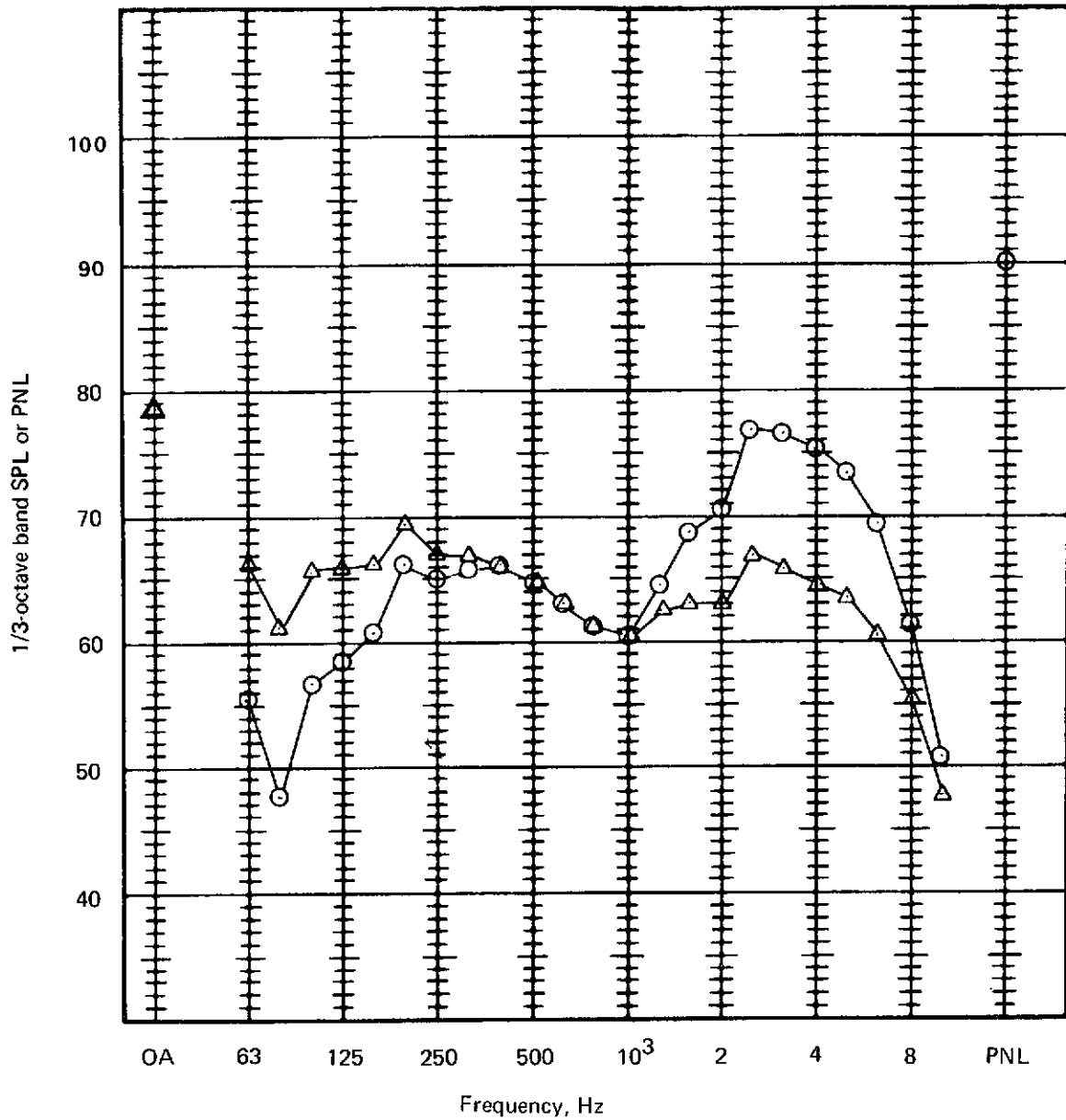
$\Delta P/P_t$, %
(Duct loss)

*FIGURE 25.—500-FT SIDELINE MAXIMUM AUGMENTOR NOISE LEVELS
FOR AN AIRCRAFT WITH WING ASPECT RATIO = 7.5*

39

Δ Physical spectrum 1/3-octave band SPL (dB re: 0.0002 microbar)
O Psychological (noy weighted) spectrum, 1/3-octave band PNL (PNdB)

Data base:

Run No. 2083, $\beta = 75°$, $\theta = 130°$, NPR = 2.6, $T_T = 300°F$,
20-lobe corrugated nozzle, valveless configuration,
$L/h_E = 55$, lining IV, $\delta_t = 10°$, H/P = 1.6, $A_3/A_1 = 11$

FIGURE 26.—500-FT SIDELINE MAXIMUM PNL TAKEOFF SPECTRA
FOR SELECTED AIRCRAFT CONFIGURATION

5.0 CONCLUSIONS

1) A valveless augmentor wing system can be designed with the same type of nozzles, flaps, and linings that are used in the task V designs having diverter valves.

2) The valveless design can utilize only limited precanting of the nozzles. The resulting increase in flow turning angle causes some loss in augmentation.

3) The task VII augmentor entrains most of its secondary air from the upper surface and tends to restrict air from the lower surface. This results in a static performance penalty which increases with higher flow turning angles.

4) The effects of 2) and 3) above are a takeoff augmentation ratio of 1.2, compared to the 1.3-value achieved with the task V AW configuration.

5) The double-layer acoustic lining tested had 3 PNdB less suppression than predicted. From the experience gained, it is believed that the suppression originally predicted is achievable.

6.0 REFERENCES

1. Roepcke, F.; and Kelly, G.: Design Integration and Noise Studies for Jet STOL Aircraft, Final Report, Vol. II, System Design and Evaluation Studies, D6-40552-2, The Boeing Company, NASA CR-114472 (originally issued as CR 114284), May 1972.

2. Campbell, J.; Lawrence, R.; and O'Keefe, J.: Design Integration and Noise Studies for Jet STOL Aircraft, Final Report, Vol. III, Static Test Program, D6-40552-3, The Boeing Company, NASA CR 114473 (originally issued as CR 114285), May 1972.

3. Campbell, J. M.; et al: Design Integration and Noise Studies for Jet STOL Aircraft, Final Report, Task V, Noise Suppression of Improved Augmentor for Jet STOL Aircraft, D6-60174, The Boeing Company (NASA CR-114534), January 1973.

4. Design Integration and Noise Studies for Jet STOL Aircraft, Task VIIA, Augmentor Wing Cruise Blowing Valveless System, Vol, II, Design Exploration, D6-40829 (NASA CR-114570), April 1973.

5. Design Integration and Noise Study for a Large STOL Augmentor Wing Transport, Task I Report, D6-60139, The Boeing Company, July 1971.

6. Wang, T.; Wright, F.; and Mahal, A.: Design Integration and Noise Studies for Jet STOL Aircraft, Final Report, Vol. IV, Wind Tunnel Test Program, D6-40552-4, The Boeing Company (NASA CR-114286), May 1972.

7. Dunn, D. G.; and Peart, N. A.: Aircraft Noise Source and Contour Estimation, D6-60233, The Boeing Company (NASA CR-114649), July 1973.